ZAMM Journal of Applied Mathematics and Mechanics
Zeitschrift für Angewandte Mathematik und Mechanik

https://onlinelibrary.wiley.com/journal/15214001

Editor: Prof. Dr. Stefan Odenbach - *Fluid Mechanics,* Professur für Magnetofluiddynamik Technische Universität Dresden.

Impact factor:1.603

Online ISSN:1521-4001

Accepted October 26th 2021

HALL AND IONSLIP EFFECTS ON NANOFLUID TRANSPORT FROM A VERTICAL SURFACE: BUONGIORNO'S MODEL

P. Ramesh Reddy[1], *S. Abdul Gaffar*[2]*, *O. Anwar Bég*[3], *B. Md. Hidayathulla Khan*[4]

[1]*Department of Mathematics, Madanapalle Institute of Technology & Sciences, Madanapalle, India*

[2]*Department of Information Technology, Mathematics Section, University of Technology and Applied Sciences, Salalah, Oman.*

[3]*Multi-Physical Simulation, Aeronautical/Mechanical Engineering Division, University of Salford, M5 4WT, UK*

[4]*Department of Mathematics, Aditya College of Engineering, Madanapalle, India*

Corresponding Author: *abdulsgaffar0905@gmail.com

Abstract

The non-linear, non-isothermal, magnetohydrodynamic (MHD) laminar convection flows of Buongiorno's nanofluid past a vertical surface with Darcy-Forchheimer model is mathematically investigated in the present article. Keller's Box implicit finite difference technique is utilized to solve the dimensionless conservation equations. Graphical and tabulated results are analyzed to study the behavior of primary and secondary velocity, temperature, nanoparticle volume fraction, shear stress rate, heat transfer rate and mass transfer rate for various emerging thermos-physical parameters. The Hall current and ion slip current effects are also considered. Validations of earlier solutions in the literature is also included. The study finds applications in nanomaterial fabrication processing, biomedical, polymer processing, chemical engineering, crude oil purifying, etc.

Keywords

Buongiorno's Nanofluid model, Heat Transfer, Hall Current, Ionslip Current, Keller-box implicit code, Mass Transfer, Nusselt number, Sherwood number.

INTRODUCTION

Nanoparticles enhance the heat transport characteristics in comparison to the regular fluid suspension, millimeter and micrometer estimated particles. In last few decades, considerable attention is paid towards Nanofluids due to its thermal performance. Experimentally, it is observed that the Nanofluid thermal quality depends on various elements such as particle material, volume fraction, particle shape and size, temperature and fluid base material. The substances added and Nanofluid sharpness helps in improving the thermal conductivity. Nanomaterial transport depends on characteristics such as size, particle shape, surfactant, combination of mixture, slip mechanisms and etc. Nanomaterials have many applications such as pharmacological methods, fuel chambers, hybrid electrical engines, automotive cooling engines, caloric control, local refrigerators, crushing processes, mining and boiler gas outlets, temperature control and microelectronics. In comparison to base fluid, these fluids maintain characteristics of increasing thermal conductivity as well as convective heat coefficient. Nanofluids are a new class of heat transfer fluids based on nanotechnology. The nanofluid is a fluid that contains particles of nanometer size. Choi [1] coined the term nanofluid as an advanced type of fluid containing particles that are smaller than 100 nm in diameter (i.e., metals, nitrides, carbides, and nanotubes (single or multiwalled)). Researchers have been motivated by the rapid growth of nanofluids use in a number of engineering fields viz. cancer therapy, finer coolants in nuclear reactors and computers, various electronic devices in military [2], oil and water [3, 4], rapid spry cooling, the food industry, vehicles and transformers, polymer extrusion, safe operations, quenching in foundries, and glass blowing [5] to investigate various aspects of nanofluid flow past different geometries. In engineering, Nanofluids are considered the best coolants. The doping of working fluid with very small solid particles for thermal engineering systems has emerged in recent years as a common technique. Vusi *et al* [6] investigated the nonlinear radiation and chemical reaction effects on double-dispensed bioconvection for Casson nanofluid flow past a stretching sheet with suction/injection. Abbas *et al*. [7] explored the slip effects on nanofluid flow in a channel with a porous wall and two different base fluid flowing in. Using Berman's similarity transformations the flow equations are simplified and solved using HAM, DTM and RK method. Sami *et al*. [8] theoretically presented the rheological characteristics of viscoelastic magnetized micropolar nanofluid with variable thermal conductivity along a moving stretched surface in the presence of gyrotactic microorganisms. Bhatti and Efstathios [9] studied the impacts of Arrhenius activation energy and viscous dissipation on the nanofluid flow of thermo-bioconvection past a riga plate considering the electromagnetic energy. The nonlinear coupled differential equations are numerically solved using shooting technique.

In many engineering and manufacturing processes, the features of magnetohydrodynaimcs (MHD) fluid flow play a critical role. Such processes include nuclear reactor design, liquid metal cooling systems, flow meters, pumps and MHD generators, etc [10]. It is also used to monitor the diffusion rate of neutrons in the thermal nuclear reactors. The electromagnetic body forces can be applied to control the fluid flow that are performed electrically thereby compensating for the momentum deficiency in the boundary layer. The unavoidable and complex applications of MHD Nanofluids (e.g., wound care, gastric medicines, targeted medication release, sterilized instruments, magnetic resonance imaging (MRI), asthma treatment, and tumor removal with hyperthermia) have attracted the attention of researchers in the study of Nanofluid related fields [11]. In strong magnetic field, the hall current and ionslip effects are important and can greatly affect the current density in hydromagnetic heat transfer. Viscous dissipation effects are also produced in many industrial and geophysical flows due to internal friction in viscous fluids which can affect temperature distribution. Various complex phenomena such as Alfven waves in plasma flows, ion-slip effects, joule heating, etc. (Cramar and Pai [12]) are generated by magnetic field in the flows of liquid with electrical conductive nature like Hall currents. The modern magnetohydrodyanmics under the strong electric field is not valid in case of ionized gases. For an ionized gas which have small density and very high magnetic field, the normal conductivity to the magnetic field is decreased due to the free spiraling of electrons and ions along the magnetic lines of force before colliding and a current is therefore generated is induced in normal to both electric and magnetic fields. This phenomenon is known as the Hall Effect. The influence of Hall and ion slip currents is therefore critical, as they have an outstanding impact on current density. Hall and ion-slip currents have a wide range of applications, especially when it comes to heat transfer, such as magnetic resonance imaging (MRI), cancer therapy, magnetic drug targeting, hall accelerators, heating elements, refrigeration coils and power generators and etc. [13]. This helps to generate artery images to evaluate the resumption of stenos or any other condition in the brain arteries and blood pumping. In addition, the analysis of the effect of the magnetic field in combination by means of Hall and ion slip effect on the blood flow in vein was found to be very beneficial and valid in magnetic resonance angiography (MRA) [14]. Mahdy *et al.* [15] reported the numerical analysis of entropy generation of viscoplastic nanofluid through a revolving sphere in a double diffusive MHD mixed convection. Asha and sunitha [16] dealt with the radiation and hall effects on peristaltic blood flow with double diffusive convection of gold nanoparticles through an asymmetric channel under the assumption of long wavelength and low Reynolds number. Devi *et al*. [17] focused on analyzing both flow and heat transport in the presence of an aligned magnetic field in an oblique Casson nanofluid past a sheet which stretches in both directions along the x-axis with heat generation by using shooting technique. Quyen *et al*. [18] tested the Lattice Boltzmann method alongside the generalized power law model for simulating non-Newtonian power-law nanofluid magnetohydrodynamics flow inside a channel with local symmetric restriction. Abiodun *et al.* [19] considered the chemically radiative mhd mixed convective Casson fluid flows through infinite vertical plates considering the effects of viscous dissipation and hall current. Singh *et al.* [20] considered the effects of Hall and ion slip currents to analyze the unstable mixed convection hydromagnetic flow of a viscoelastic fluid past a vertical porous channel. Ibrahim and Anbessa [21] explored the casson nanofluid's radiative 3D MHD mixed convection flow past an exponentially stretching sheet considering the Hall and ion slip effects and heat source.

Viscous dissipation plays a significant role in laminar convection, geological processes, polymer processing and large scale strong gravitational field. The viscous dissipation causes variation in temperature and affects the heat transfer rate. Viscous dissipation or internal friction is the rate of work done against the viscous forces that are irreversibly converted into internal energy. Joule heating has always been one of the fascinating effects to impose as it gives strong impact to the MHD flow of fluids. Joule or Ohmic heating is the process of converting electric energy into thermal energy which evolves heat through material resistances. Consequently, in most electronic and electrical devices, the Joule heating effect is broadly and virtually utilized. This interested us to impose joule heating term, which is customarily overlooked mostly on assumption that Eckert number is small under normal conditions based on the order of the magnitude analysis. The viscous dissipation and Joule heating or ohmic heating effects are typically identified by the Eckert number and the product of the Eckert number and magnetic parameter, respectively. Ahmed *et al*. [22] examined Soret-Dufour's mechanism of both positive and negative effects with heat and mass transfer processes over an advancing permeable surface by using the spectral homotopy analysis approach to understand the buoyancy force and viscous dissipation effects. Ibrahim and Gadisa [23] investigated the effects of viscous dissipation and unstable parameters on nonlinear convective laminar boundary layer flow of micropolar-couple stress nanofluid in the presence of suction/injection vector, through a permeable stretching sheet with non-Fourier heat flux model. Nagaraju and Mahesh [24] presented the effects of viscous dissipation and internal heat source on the mixed convection stagnation point couple stress nanofluid past a stretched cylinder of variable thermal conductivity. Safwa *et al.* [25] presented the effects of Joule heating MHD convection flows of hybrid nanofluid past a shrinking cylinder. Usman *et al*. [26] examined the non-isothermal heat transfer of a magnetohydrodynamic micropolar nanofluid past a non-linear extended wall, taking into account Brownian motion and thermophoresis, coupled stress, hall current and viscous dissipation effects.

Convection fluid flows in porous media have prominent mechanical and petroleum engineering applications. For instance, geothermal supply, nuclear wastages, substerranean rapid spreading of substance abuse, grain collection, modified oil storage, oil production restoration, Co_2 sequester, and so on [27 – 29]. Darcy suggested a pre-empirical equation which pioneered. In semi-analytical equation, nonlinearity exists for large Reynolds number which attributed to increasing role of inertial forces. High velocities describe many modern applications of porous media. The non-Darcian porous media is a modified version of the classical Darcy law that considers the effects of porosity and inertia. Darcy's classical principal isn't valid for greater velocities and porosities. Forchheimer [30] thereby considered the effects of inertia by including a square term of velocity in momentum equation. Later, Muskat [31] has designated this factor as "Forchheimer's term" which always holds for high Reynolds number. Owing to the rotation of a disk with partial slip conditions, the Darcy-Forchheimer flux of water-based nanofluids was Hayat *et al.* [32] using optimal homotopic analysis method. They also considered the effects of viscous dissipation. Sohail *et al.* [33] investigated the Sisko nanofluid's optimization of entropy generation and nonlinear radiative mhd flow through a rotating disk with non-Darcy porous medium in the presence of Joule heating and non-uniform source/sink heat. Anwar *et al.* [34] investigated the thermal properties of the Darcy-Forchheimer hydromagnetic hydbrid nanofluid flow through a permeable stretching cylinder.

The Nanofluid flow study with MHD and Hall/Ionslip current is a vital application in both science and engineering. Therefore, in the present study we analyze the steady MHD convection flows of Nanofluid with Hall/Ionslip current and viscous dissipation effects from a vertical surface. The governing conservation equations for mass, linear momentum, energy and nanoparticle volume fraction with associated boundary conditions are transformed to dimensionless coupled partial differential boundary value problem. The nonlinearity of the emerging model does not permit exact solutions and therefore an implicit finite difference computational method (Keller's box scheme) [35] is utilized. The present Keller-Box results are validated with the earlier Newtonian studies [36–40] available in the literature. The study finds applications in heat exchangers technology, materials processing and geothermal energy storage etc.

MATHEMATICAL MODEL

A laminar, steady-state, incompressible, partially-ionized, electrically conduction laminar convection flow of Nanofluid past an inclined rigid sheet in an (x, y, z) coordinate system is studied, as illustrated in Fig. 1. The sheet is inclined at an angle, Ω, to the horizontal. For the partially ionized fluid, the magnetic Reynolds number is small, so the magnetic induction effect can be overlooked. The relative motion of the fluid particles, however, will occur and it is presumed that the frequency of the electron-atomic collision is high enough for Hall and ionslip currents to be relevant. As such, the relative motion of charged particles must be measured by an electrical current density, J. The generalized Ohm law can be utilized in order to consider only the electromagnetic forces on certain particles. On applying a magnetic field, normal to the electrical field, an electromagnetic force is produced normally in the z direction. Such a force induces a perpendicular movement of charged particles in both magnetic and electrical fields [12]. A part of electrical current density therefore exists normal to both magnetic and electrical fields and this signifies the Hall current. The diffusion velocity of the ions would be important for a strong magnetic field, which constitutes the effect of ionslip. Therefore, the equation of conservation of electrical charge is:

$$\nabla .\ J = 0 \tag{1}$$

Where $J = \left(J_x, J_y, J_w\right)$. Since the vertical surface is not made up of electrically conductive material, electrical charge at the vertical surface is constant and zero i.e., $J_y \to 0$. Hence, we conclude that $J_y = 0$ throughout the fluid regime in the porous medium. The magnetic field acts in y-direction with B_0 as its component. Both Nanofluid and vertical surface are initially maintained at a constant temperature and concentration. And the fluid temperature and concentration are elevated to the ambient fluid temperature and concentration that remain unchanged. A homogeneous and isotropic porous medium is assumed in order to simulate the hydraulic conductivity. The pressure gradient of the second order Darcy-Forchheimer model is defined as:

$$\nabla p = -aU + bU^2 \tag{2}$$

Where ∇p is the pressure, $a = \frac{\mu}{K}$ and $b = \frac{\rho}{K_1}$ are the constants and U is the velocity.

Further under usual boundary layer and Boussinesq approximation the relevant boundary layer equations of an incompressible Buongiorno's nanofluid [41] are as follows:

$$\nabla.\, \mathrm{V} = 0 \tag{3}$$

$$\rho_f\left(\frac{\partial \mathrm{V}}{\partial t} + \mathrm{V}.\nabla\mathrm{V}\right) = -\nabla p + \mu\nabla^2\mathrm{V} + g\left[\left(1 - C_\infty\right)\rho_{f\infty}\beta\left(T - T_\infty\right) - \left(\rho_p - \rho_{f\infty}\right)\left(C - C_\infty\right)\right] + J \text{ x } B \tag{4}$$

$$\left(\rho c\right)_m\left(\frac{\partial T}{\partial t} + \mathrm{V}.\nabla\mathrm{T}\right) = k_m\nabla^2 T + \varepsilon\left(\rho c\right)_m\left[D_B\nabla C.\nabla T + \frac{D_T}{T_\infty}\left(\nabla T\right)^2\right] \tag{5}$$

$$\frac{\partial C}{\partial t} + \frac{1}{\varepsilon}\mathrm{V}.\nabla C = D_B\nabla^2 C + \frac{D_T}{T_\infty}\nabla^2 T \tag{6}$$

The generalized Ohm's law [42] with Hall and ion-slip effects is given by:

$$J = \sigma\left(E + V \text{ x } B\right) - \frac{\beta_e}{B_0}\left(J \text{ x } B\right) + \frac{\beta_e\beta_i}{B_0^2}\left(J \text{ x } B\right) \text{ x } B \tag{7}$$

$$\nabla.B = 0 \tag{8}$$

$$\nabla \text{ x } H = J \tag{9}$$

$$\nabla \text{ x } E = 0 \tag{10}$$

We write $V = \left(u, v, w\right)$ and $\beta_e = \omega_e\tau_e$ and $\beta_i = \omega_i\tau_i$. The current density vector, using Maxwell equation can be written as:

$$J = \frac{\sigma B}{\left(1 + \beta_i\beta_e\right)^2 + \beta_e^2}\left(\beta_e u - \left(1 + \beta_i\beta_e\right)w, 0, \left(1 + \beta_i\beta_e\right)u + \beta_e w\right) \tag{11}$$

Further, Eqn. (9), the Lorentz force can be written as:

$$J \times B = \frac{\sigma B^2}{\left(\left(1 + B_i B_e\right)^2 + B_e^2\right)}\left(-\left(1 + B_i B_e\right)u - B_e w, 0, B_e u - \left(1 + B_i B_e\right)w\right) \tag{12}$$

The associated boundary conditions on the cone surface (wall) and in the free stream (edge of the boundary layer) are:

$$\begin{aligned} &u = v = 0, \quad w = 0, \quad T = T_w, \quad C = C_w \qquad at \quad y = 0 \\ &u \to 0, \quad w \to 0, \quad T \to T_\infty, \quad C \to C_\infty \qquad at \quad y \to \infty \end{aligned} \tag{13}$$

With the Oberbeck-Boussinesq approximation, the linearized momentum equation is:

$$0 = -\nabla p + \mu \nabla^2 \mathrm{V} + g\left[\left(1 - C_\infty\right)\rho_{f\infty}\beta\left(T - T_\infty\right) - \left(\rho_p - \rho_{f\infty}\right)\left(C - C_\infty\right)\right] + J \text{ x } B \tag{14}$$

The governing equations:

$$\frac{\partial u}{\partial x} + \frac{\partial v}{\partial y} = 0 \tag{15}$$

$$\begin{aligned} u\frac{\partial u}{\partial x} + v\frac{\partial u}{\partial y} = \nu\frac{\partial^2 u}{\partial y^2} + \left[\left(1 - C_\infty\right)\rho_{f\infty}\beta\left(T - T_\infty\right) - \left(\rho_p - \rho_{f\infty}\right)\left(C - C_\infty\right)\right]g - \frac{\nu}{K}u - \frac{b}{K}u^2 \\ - \frac{\sigma B_0^2}{\rho\left(\alpha_e^2 + \beta_e^2\right)}\left(\alpha_e u + \beta_e w\right) \end{aligned} \tag{16}$$

$$u\frac{\partial w}{\partial x} + v\frac{\partial w}{\partial y} = \nu\frac{\partial^2 w}{\partial y^2} - \frac{\nu}{K}w - \frac{b}{K}w^2 + \frac{\sigma B_0^2}{\rho\left(\alpha_e^2 + \beta_e^2\right)}\left(\beta_e u - \alpha_e w\right) \tag{17}$$

$$u\frac{\partial T}{\partial x} + v\frac{\partial T}{\partial y} = \alpha_m\frac{\partial^2 T}{\partial y^2} + \tau\left[D_B\frac{\partial T}{\partial y}\frac{\partial C}{\partial y} + \frac{D_T}{T_\infty}\left(\frac{\partial T}{\partial y}\right)^2\right] + \frac{\nu}{c_p}\left(\left(\frac{\partial u}{\partial y}\right)^2 + \left(\frac{\partial w}{\partial y}\right)^2\right) + \frac{\sigma B_0^2}{\rho c_p\left(\alpha_e^2 + \beta_e^2\right)}\left(u^2 + w^2\right) \tag{18}$$

$$\frac{1}{\varepsilon}\left(u\frac{\partial C}{\partial x} + v\frac{\partial C}{\partial y}\right) = D_B\frac{\partial^2 C}{\partial y^2} + \frac{D_T}{T_\infty}\frac{\partial^2 T}{\partial y^2} \tag{19}$$

Where $\alpha_m = \dfrac{k_m}{(\rho c)_f}, \quad \tau = \dfrac{(\rho c)_p}{(\rho c)_f}, \quad \alpha_e = 1 + \beta_i\beta_e.$ (20)

The relevant boundary conditions imposed at the plate surface and in the free stream:

$$\begin{aligned} &u = v = 0, \quad w = 0, \quad T = T_w, \quad C = C_w \qquad at \quad y = 0 \\ &u \to 0, \quad w \to 0, \quad T \to T_\infty, \quad C \to C_\infty \qquad at \quad y \to \infty \end{aligned} \tag{21}$$

Eqn. (15) is automatically satisfied subject to the velocity components expressed in terms of stream function ψ as $u = \dfrac{\partial \psi}{\partial y} \quad and \quad v = -\dfrac{\partial \psi}{\partial x}$.

The following dimensionless quantities are introduced:

$$\xi=\left(\frac{x}{L}\right)^{\frac{1}{2}},\quad \eta=\frac{C_1 y}{x^{\frac{1}{4}}},\quad \psi=4\nu C_1 x^{\frac{3}{4}} f(\xi,\eta),\quad w=4\nu C_1^2 x^{\frac{1}{2}} g(\xi,\eta)$$

$$\theta(\xi,\eta)=\frac{T-T_\infty}{T_w-T_\infty},\ \phi(\xi,\eta)=\frac{C-C_\infty}{C_w-C_\infty},\quad C_1^4=\frac{(1-C_\infty)\rho_{f\infty} g\beta(T_w-T_\infty)}{4\nu^2} \tag{22}$$

Eqns. (16) - (19) are thereby rendered into the following coupled nonlinear partial differential boundary layer equations:

$$f'''+3ff''-2f'^2+(\theta-Nr\phi)-\frac{2\xi^4}{Da\,Gr^{1/2}}f'-\frac{4\ Fs}{Da}\xi^2 f'^2-\frac{2Ha}{\alpha^2+\beta^2}\xi\left(\alpha_e f'+\beta_2 g\right)=2\xi\left(f'\frac{\partial f'}{\partial\xi}-f''\frac{\partial f}{\partial\xi}\right) \tag{23}$$

$$g''+3fg'-2f'g-\frac{2\xi^4}{Da\,Gr^{1/2}}g-\frac{4\ Fs}{Da}\xi^2 g^2+\frac{2Ha}{\alpha^2+\beta^2}\xi\left(\beta_2 f'-\alpha_e g\right)=2\xi\left(f'\frac{\partial g}{\partial\xi}-g'\frac{\partial f}{\partial\xi}\right) \tag{24}$$

$$\frac{\theta''}{\Pr}+3f\theta'+Nb\,\theta'\phi'+Nt\,\theta'^2+4Ec\xi^2\left(f''^2+g'^2\right)+\frac{8Ha.Ec}{\alpha^2+\beta^2}\xi^3\left(f'^2+g^2\right)=2\xi\left(f'\frac{\partial\theta}{\partial\xi}-\theta'\frac{\partial f}{\partial\xi}\right) \tag{25}$$

$$\frac{\phi''}{Le}+3f\phi'+\frac{1}{Le}\frac{Nt}{Nb}\theta''=2\xi\left(f'\frac{\partial\phi}{\partial\xi}-\phi'\frac{\partial f}{\partial\xi}\right) \tag{26}$$

The transformed non-dimensional boundary conditions are:

$$\begin{aligned} &f=0,\quad f'=0,\quad g=0,\quad \theta=0,\quad \phi=0 \quad at\ \ \eta=0\\ &\qquad\quad f'\to 0,\quad g\to 0,\quad \theta\to 0,\quad \phi\to 0 \quad at\ \ \eta\to\infty \end{aligned} \tag{27}$$

Here

$$Nr=\frac{(\rho_p-\rho_{f\infty})(C_w-C_\infty)}{\rho_{f\infty}(1-C_\infty)\beta(T-T_\infty)},\quad Gr=\frac{(1-C_\infty)\rho_{f\infty}g\beta(T_w-T_\infty)L^3}{\nu^2},\quad Ha=\frac{\sigma B_0^2 L^{1/2}}{2\rho\nu C_1^2},\ Da=\frac{K}{L^2}$$

$$Fs=\frac{b}{L},\ Nb=\frac{\tau D_B(C_w-C_\infty)}{\nu},\ Nt=\frac{\tau D_T(T_w-T_\infty)}{\nu T_\infty},\ \Pr=\frac{\nu}{\alpha_m},\ Le=\frac{\nu}{D_m\varepsilon},\ Ec=\frac{4L\nu^2C_1^4}{c_p(T_w-T_\infty)} \tag{28}$$

The engineering parameters at the plate surface, the skin-friction coefficient (C_{fx} *and* C_{fz}) (shear stress at the surface along x and z directions), Nusselt number (Nu), (heat transfer rate) and Sherwood number (Sh) (mass transfer rate) are defined as follows:

$$C_{fx} = \sqrt{2}\mu\nu \frac{Gr_x^{3/4}}{x^2} f''(\xi,0) \tag{29}$$

$$C_{fz} = \sqrt{2}\mu\nu \frac{Gr_x^{3/4}}{x^2} g'(\xi,0) \tag{30}$$

$$Nu = -\frac{1}{\sqrt{2}} Gr_x^{-\frac{1}{4}} \theta'(\xi,0) \tag{31}$$

$$Sh = -\frac{1}{\sqrt{2}} Gr_x^{-\frac{1}{4}} \phi'(\xi,0) \tag{32}$$

NUMERICAL SOLUTION

The dimensionless Eqns. (23) - (27) are numerically solved using Keller's Box implicit finite difference scheme that is comparatively more effective and powerful then numerous mathematical techniques and accumulates more quickly with second order accuracy. This method provides an improvement in accuracy on explicit or semi-implicit schemes and utilizes customizable stepping in a fully implicit approach. The Keller-Box discretization is fully coupled at each step which reflects the physics of parabolic systems. The discrete calculus of the Keller-Box technique is fundamentally different from all other numerical techniques. In Table 1, the present results of local skin friction coefficient (C_{fx}) are compared with Newtonian solutions presented by Pozzi and Lipo [43], Merkin and Pop [44] and Saddiqa *et al.* [45] for various values of ξ and excellent agreement is achieved.

RESULTS AND DISCUSSION

The present section highlights the physical perspective of Hall and ion slip current effects on Buongiorno's Nanofluid flow past a vertical surface. The Keller-box finite difference results of equations (23) – (27) as velocity, temperature, nanoparticle volume fraction concentration as well the shear stress rate, heat transfer rate and nanoparticle mass transfer rate for various values of the dimensionless thermophysical parameters viz., *nanoparticle Brownian motion parameter* (*Nb*), *thermophoresis parameter* (*Nt*), *buoyancy ratio parameter* (*Nr*), *Hartmann number* (*Ha*), *Hall current* (β_e), *ion slip current* (β_i), *Eckert number* (*Ec*), *Darcy number* (*Da*) and *Forchheimer number* (*Fs*) are presented along the radial coordinate (η) in form of tables and figures. The skin friction coefficients (C_{fx} and C_{fz}), heat transfer coefficient (*Nu*) and mass transfer rate (*Sh*) for different values of Nb, Nt, β_e, β_i, Ec, Da, Ha and Fs are depicted in Table 2 – 9. Clearly, a slight increase in C_{fx} and C_{fz} is observed for various values of Nb. Whereas, Nu is reduced. And a significant increase in Sh is observed. Also, an increase in Nt is seen to increase C_{fx} and C_{fz} slightly while Nu and Sh are reduced. Further, C_{fx}, C_{fz} and Sh are lowered with increasing β_e values whereas Nu is increased. Increasing β_i, is observed to increase C_{fx}, C_{fz} Nu and Sh. Also, it is observed that increasing Ha is seen to increase C_{fx}, C_{fz}, Nu and Sh. The heat flow from the fluid to the plate leads to higher heat transfer rate and a decrease in fluid temperature. A significant increase in C_{fx} and Sh is observed with an increase in Ec. While Nu is reduced and a slight decrease is observed in C_{fz}. Also, the C_{fx}, C_{fz} and Nu are enhanced with an increase in Da whereas Sh is reduced. Further,it is observed that the C_{fx} and C_{fz} are reduced for increasing values of Fs. Whereas Nu and Sh are enhanced.

Figs. 2(a) - 2(d) illustrates the velocity, temperature and nanoparticle volume fraction concentration profiles for various values of hall current, β_e over the plate regime. The production of potential difference is the Hall current. A significant rise in primary velocity profiles is observed with an increase in β_e values. In magnetohydrodynamics, the parameter β_e causes a cross flow phenomenon. The addition of the parameter β_e decreases the effective conductivity and thereby lowers the resistive magnetic force. The primary velocity converges asymptotically to diminishing free stream velocity in all situations. The secondary velocity, temperature and nanoparticle concentration are reduced with increasing β_e values. Thereby, the thermal and concentration boundary layer thickness is also reduced. The secondary velocity is maximum closer to the plate surface. The thermal and concentration boundary layers are cooled and their thickness is reduced as the β_e increases. The Hall parameter plays a crucial role in nanofluid flow. The magnetic damping force is reduced because the effective conductivity is reduced. Longitudinal Hall current contributes a transverse body force to the flow, causing a transverse velocity gradient.

Figs. 3(a) - 3(d) illustrates the velocity, temperature and nanoparticle volume fraction concentration profiles for various values of ion slip current, β_i over the plate regime. A significant raise in primary velocity profiles is observed with an increase in β_i values. The secondary velocity, temperature and nanoparticle concentration are reduced with increasing β_e values. Thereby, the thermal and concentration boundary layer thickness is also reduced. As the ionslip current increases the effective conductivity of the fluid increases and therefore the damping force decreases and hence the non-dimensional velocity increases. As the ions slip in the magnetic field, the ionslip parameter causes a heating effect on the secondary flow as well as a slowdown. The ionslip effect has positive effect only on the primary flow, which is advantageous in MHD energy generation systems. It's also worth noting that values of primary velocity are typically several orders of magnitude greater than secondary velocity, which is a common occurrence in MHD flows.

Figs. 4(a) - 4(d) illustrates the velocity, temperature and nanoparticle volume fraction concentration profiles for various values of *Nb* over the plate regime. A significant raise in primary and secondary velocity profiles is observed with a significant change in *Nb* values. A gradual increase in fluid temperature is observed with a rise in *Nb* values. Which is due to the hotter particles force the smaller particles move towards the cooler surface. Also, the enhanced random motion of the fluid particles elevate fluid temperature. However, the nanoparticle concentration is significantly reduced. The rearrangement of nanoparticle form a new structure due to random diffusivity and hence the nanofluid's thermal conductivity increases.

Fig. 5(a) – 5(d) depicts the effect of *Nt* on velocity, temperature and nanoparticle volume fraction concentration along the vertical surface regime. Thermophoresis is a phenomenon that transfers the particles so that the fluid temperature compresses due to temperature gradient. The parameter *Nt* plays a significant role in temperature diffusion and volume fraction of the nanoparticle. As *Nt* increases, a slight decrease in primary and secondary velocity of is observed. Conversely, the temperature and volume fraction are gradually increased. As *Nt* increases, the heat transfer in the boundary layer increases and at the same time exacerbates particle deposition away from the fluid field, thus increasing volume fraction of the nanoparticles as shown in Fig. 5(c). Greater thermophoresis suggests lasting motion of nanoparticles with respect to the rate of heat transfer away from the surface. Due to increasing *Nt* values, smaller particles are pulled towards the cooler area, thereby reducing the fluid concentration. Hence the thermal and Nanofluid volume fraction boundary layers are enhanced. The thermophoresis and Brownian motion parameters are the most interesting features supported for Buongiorno's nanofluid model. Such parameters essentially increase the fluid temperature. With increasing *Nb* values, the Brownian motion of the fluid is greatly effects due to random motion of the nanoparticles. In addition, the thermophoresis achieves a gradual transfer of nanoparticles from hotter region towards the colder region and hence the temperature increases. A gradually increase in Nt contributed to greater mass flux due to the temperature gradient and hence the nanoparticle concentration increases.

Figs. 6(a) - 6(d) displays the effects of *Hartmann number, Ha,* on the velocity, temperature and nanoparticle volume fraction respectively. The primary velocity is observed to diminish as the Ha values increase. Whereas the secondary velocity is enhanced greatly with a rise in Ha values. The transverse magnetic field applied normal to the flow direction gives rise to the resistance force called Lorentz force. Therefore, with applied magnetic field the Lorentz force emerges and opposes the flow and hence the fluid velocity decreases. The presence of magnetic term produces a drag force and hence the motion of the fluid slows down. The temperature and nanoparticle volume fraction profiles are also seen to significantly increase with an increase in Ha values. With

Figs. 7(a) – 7**(d)** depict the influence of Da velocity, temperature and nanoparticle volume fraction respectively. Clearly from figs. 7(a-b) we observe that the primary and secondary velocities are enhanced with an increases in Da values. Whereas, the temperature and nanoparticle volume fraction are reduced with increasing Da values. The gradual decline of solid fibers with high Da values in porous media helps in decreasing heat transfer of thermal conduction in the system. This restricts the diffusion of thermal energy from the vertical surface to the system and cools the thermal boundary layer thickness which decreases as well. Therefore, the existence of porous media causes a substantial impact in the momentum and thermal diffusion of the system, providing a strong framework for thermal regulation and flow control. From eqn. (23), we can see that the Darcian bulk impedance term is inversely proportional to the Darcy number. As a result, as Da increases, the Darcian impedance, which emerges from the viscous contribution to stress at solid particle surfaces, reduces significantly. With higher Da values (more permeability), the flow encounters less matrix resistance from the porous fibers, which become less prevalent. Hence as Da increases, the flow accelerates and primary velocity increases and the regime's momentum increases.

Figs. 8(a) – 8**(d)** depict the influence of Fs on velocity, temperature and nanoparticle volume fraction respectively. The primary and secondary velocities are reduced with an increase in Fs values. Whereas, the temperature and nanoparticle volume fraction are enhanced with a rise in Fs values. Physically, the coefficient of inertia is correlated with the drag force and hence an increase in inertia generates more drag force in the fluid which gradually decreases the fluid velocity. The quadratic inertial drag has a greater impact closer to the wall. Nevertheless, Forchimmer drag is of order two and an increase in *Fs* essentially plains the momentum development and hence decelerates the flow.

Figs. 9(a) – 9**(d)** depict the influence of Eckert number, *Ec* on velocity, temperature and nanoparticle volume fraction respectively. For larger values of *Ec*, primary velocity, secondary velocity and temperature profiles are seen to increase whereas the nanoparticle concentration is seen to decrease. According to Schlichting [46], Eckert number is the ratio of the flow's kinetic energy to the boundary layer enthalpy difference. The Eckert number is used in high-altitude rocket aerothermodynamics. It refers to the difference between total mechanical power input and the lower amount of total power input that produces thermodynamically reversible effects, such as kinetic and potential energy elevations, in low-speed incompressible flows. The energy dissipated as thermal energy by viscous effects i.e., the work done by the viscous fluid in overcoming internal friction, is referred to as viscous heating. Plate cooling, i.e. heat loss from the plate to the fluid corresponds to positive *Ec* values, whereas plate heating, i.e. heat gain from the fluid, corresponds to negative *Ec* values. Physically, a rise in *Ec* values tend to raise the thermal profile and the frictional heat generation. Hence the fluid moves faster along the surface and leads to growth in particle temperature.

CONCLUDING REMARKS

The Darcy-Forchheimer MHD convection flow of Buongiorno's Nanofluid from a vertical surface is investigated numerically in the present paper. The finite difference Keller's box technique is employed to solve the transformed nonlinear problem with associated wall and free stream boundary conditions. Furthermore, the Keller box numerical solutions are validated with the previous Newtonian studies. The observations of the present study are as follows:

i. Increasing β_e and β_i induces a rise in primary velocity distributions whereas secondary velocity, temperature and nanoparticle volume fraction are reduced.
ii. As *Nb* increases the primary and secondary velocities and temperature distributions are seen to increase whereas nanoparticle concentration decreases.
iii. As *Nt* increases primary and secondary velocities are decreased whereas temperature and nanoparticle concentration are increased.

iv. With increasing *Nr*, the primary skin friction, secondary skin friction, heat transfer rate and mass transfer rate are reduce.

v. It is evident that increasing *Ha* reduces primary velocity but increases secondary velocity, temperature and concentration profiles.

NOMENCLATURE

B_0	*Imposed magnetic field*	U	*Velocity*
B	*Magnetic field*	V	*Velocity vector*
a	*Constant*	u, v, w	*Dimensionless velocity components in X, Y and Z direction respectively*
b	*Forchheimer inertial drag parameter*	x	*Stream wise coordinate*
C	*Nanoparticle volume fraction*	y	*Transverse coordinate*
C_{fx}, C_{fz}	*Skin Friction Coefficients*	***Greek Symbols***	
c_p	*specific heat*	α_m	*Thermal diffusivity of the Nanofluid*
D_B	*Brownian diffusion coefficient*	β	*Volumetric volume expansion coefficient of the fluid*
Dm	*Mass diffusion*	τ	*Ratio of effective heat capacity of nanoparticle to the heat capacity of the fluid*
D_T	*Thermophoretic diffusion coefficient*	σ	*Electric conductivity of the fluid*
E	*Electrical field*	η	*Non-dimensional radial coordinate*
f	*Dimensionless stream function*	μ	*Dynamic viscosity*
g	*Gravitational acceleration*	ξ	*Non-dimensional tangential coordinate*
K	*Permeability of the porous media*	ψ	*Non-dimensional stream function*
K_1	*Inertial permeability*	ν	*Kinematic viscosity*
k	*Thermal conductivity of the fluid*	ϕ	*Dimensionless concentration*
k_m	*Effective thermal conductivity*	θ	*Dimensionless temperature*
Gr_x	*Local Grashof number*	ρ_p	*Density of the fluid*
Nb	*Brownian motion parameter*	$(\rho c)_m$	*Effective heat capacity*

Nt	*Thermophoresis parameter*	ρ_f	*Density of the fluid*
Nr	*Buoyancy ratio parameter*	β_e	*Hall current parameter*
Nu	*Heat transfer coefficient*	β_i	*Ionslip parameter*
Pr	*Prandtl number*	ω_e	*electron frequency*
Le	*Lewis number*	τ_e	*Electorn collision time*
J	*Current density vector*	***Subscripts***	
Sh	*Mass transfer coefficient*	*w*	*Conditions on the wall*
T	*Fluid temperature*	∞	*Free stream condition*

REFERENCES

[1] Choi SUS, Enhancing thermal conductivity of fluids with nanoparticles. In: Siginer DA, Wang HP, eds. Developments and Applications of Non-Newtonian flows, New York, NY: ASME; 1995, 231, 99-105.

[2] Saidur, R.; Leong, K.Y.; Mohammad, H. A review on applications and challenges of nanofluids. *Renew. Sustain. Energy Rev*. 2011, 15, 1646–1668.

[3] Xiao, B.; Zhang, X.; Wang, W.; Long, G.; Chen, H.; Kang, H.; Ren, W. A fractal model for water flow through unsaturated porous rocks. *Fractals* 2018, 26, 1840015.

[4] Long, G.; Xu, G. The effects of perforation erosion on practical hydraulic-fracturing applications. SPE J. 2017, 22, 645–659.

[5] Wong, K.V.; De Leon, O. Applications of nanofluids: Current and future. Adv. Mech. Eng. 2010, 2, 519659.

[6] Vusi M. Magagula, Sachin Shaw, Rishi Raj Kairi, Double dispersed bioconvective Casson nanofluid flow over a nonlinear convective stretching sheet in suspension of gyrotactic microorganism, *Heat Transfer*, 49(15), 2449-2471, 2020.

[7] Z. Abbas, J. Hasnain, S. Aly, M. Sheikh, Comparative analysis for partial slip flow of ferrofluid Fe_3O_4 nanoparticles in a semi-porous channel, *Journal of King Saud University - Science* (2020), https://doi.org/10.1016/j.jksus.2020.05.007

[8] Sami Ullah Khan, Muhammad Mubashir Bhatti, Arshad Riaz, A revised viscoelastic micropolar nanofluid model with motile micro-organisms and variable thermal conductivity, *Heat Transfer*, 2020. https://doi.org/10.1002/htj.21797

[9] M. M. Bhatti, Efstathios E. Michaelides, Study of Arrhenius activation energy on the thermo-bioconvection nanofluid flow over a Riga plate, *J Therm Anal Calorim*, 2020. https://doi.org/10.1007/s10973-020-09492-3

[10] Sutton G W & Sherman A, Engineering Magnetohydrodynamics, Mc Graw-Hill: New York, 1965.

[11] Wahed Hasona, Nawal Almalki, Abdelhafeez ElShekhipy, Mohamed Ibrahim, Combined Effects of Thermal Radiation and Magnetohydrodynamic on Peristaltic Flow of Nanofluids: Applications to Radiotherapy and Thermotherapy of Cancer, *Current Nanoscience*, 2020, *16*, 121-134, DOI:*10.2174/1573413715666190318161351*

[12] Cramer K and Pai S, Magnetofluid Dynamics for Engineers and Applied Physicists, New York: McGraw-Hill, USA, 1973.

[13] M. Veera Krishna, Ali J. Chamkha, Hall and ion slip effects on Unsteady MHD Convective Rotating flow of Nanofluids—Application in Biomedical Engineering, *Journal of the Egyptian Mathematical Society*, (2020) 28:1 https://doi.org/10.1186/s42787-019-0065-2

[14] K. V. B. Rajakumar, T. Govinda Rao, M. Umasankara Reddy, K. S. Balamurugan, Influence of Dufour and thermal radiation on unsteady MHD Walter's liquid model-B flow past an impulsively started infinite vertical plate embedded in a porous medium with chemical reaction, Hall and ion slip current, *SN Applied Sciences* (2020) 2:742 | https://doi.org/10.1007/s42452-020-2484-y

[15] Mahdy A., Ali J Chamkha, Hossam A. Nabwey, Entropy analysis and unsteady MHD mixed convection stagnation-point flow of Casson nanofluid around a rotating sphere, *Alexandria Engineering Journal*, 2020. https://doi.org/10.1016/j.aej.2020.04.028

[16] Asha S.K. and Sunitha G., Thermal radiation and Hall effects on peristaltic blood flow with double diffusion in the presence of nanoparticles, *Case Studies in Thermal Engineering, 17*, 2020, 100560. https://doi.org/10.1016/j.csite.2019.100560

[17] Renu Devi, Vikas Poply, Manimala, Impact of aligned MHD flow with inclined outer velocity for a casson nanofluid over a stretching sheet, *Heat Transfer*, 2020, https://doi.org/10.1002/htj.21796.

[18] Quyen Nguyen, Mehdi Jamali Ghahderijani, Mehrdad Bahrami, Ehsan Kamali Ahangar, Annunziata D'Orazio, Quang-Vu Bach, Arash Karimipour5, Develop Boltzmann equation to simulate non-Newtonian magnetohydrodynamic nanofluid flow using power law magnetic

Reynolds number, *Mathematical Methods in the Applied Sciences*, 2020. https://doi.org/10.1002/mma.6513

[19] Abiodun A. Opanuga, Samuel O. Adesanya, Hilary I. Okagbue, Olasumbo O. Agboola, Impact of Hall Current on the Entropy Generation of Radiative MHD Mixed Convection Casson Fluid, *Int. J. Appl. Comput. Math* 6, 44 (2020). https://doi.org/10.1007/s40819-020-0790-0

[20] J. K. Singh, G. S. Seth, Naveen Joshi and C. T. Srinivasa, Mixed convection flow of a viscoelastic fluid through a vertical porous channel influenced by a moving magnetic field with Hall and ion-slip currents, rotation, heat radiation and chemical reaction, *Bulgarian Chemical Communications, Volume 52, Issue 1 (pp. 147-158) 2020. DOI: 10.34049/bcc.52.1.4689*

[21] Wubshet Ibrahim and Temesgen Anbessa, Three-Dimensional MHD Mixed Convection Flow of Casson Nanofluid with Hall and Ion Slip Effects, *Mathematical Problems in Engineering*, Volume 2020, Article ID 8656147, 15 pages, 2020. https://doi.org/10.1155/2020/8656147

[22] Lukman O. Ahmed, Bidemi O. Falodun, Jimoh Abdulwaheed, Mechanism of Soret-Dufour, magnetohydrodynamics, heat and mass transfer flow with buoyancy force, and viscous dissipation effects, *Heat Transfer*, 49 (5), 2831-2848. https://doi.org/10.1002/htj.21748

[23] Wubshet Ibrahim, Gosa Gadisa, Nonlinear convective boundary layer flow of micropolar-couple stress nanofluids past permeable stretching sheet using Cattaneo-Christov heat and mass flux model, *Heat Transfer*, 49(5), 2521-2550, 2020. https://doi.org/10.1002/htj.21733

[24] Nagaraju Gajjela, Mahesh Garvandha, Impacts of variable thermal conductivity and mixed convective stagnation-point flow in a couple stress nanofluid with viscous heating and heat source, *Heat Transfer*, 2020. https://doi.org/10.1002/htj.21792

[25] N. Safwa Khashi'ie, N. Md Arifin, I. Pop, N. Syahirah Wahid, Flow and heat transfer of hybrid nanofluid over a permeable shrinking cylinder with Joule heating: A comparative analysis, *Alexandria Engineering Journal* (2020), doi: https://doi.org/10.1016/j.aej.2020.04.048

[26] A. H. Usman, U. W. Humphries, P. Kumam, Z. Shah and P. Thounthong, Double Diffusion Non-Isothermal Thermo-Convective Flow of Couple Stress Micropolar Nanofluid Flow in a Hall MHD Generator System, *IEEE Access*, vol. 8, pp. 78821-78835, 2020, doi: 10.1109/ACCESS.2020.2986021.

[27] Hyder J.L. and Garrett, P.M., A theoretical model for *in situ* leaching of radionuclides from buried radioactive waste, *Nuclear and Chemical Waste Management*, 3, 149-152 (1982).

[28] Bechthold, W., E. Smailos, S. Heusermann, W. Bollingerfehr, B. Bazargan-Sabet, T. Rothfuchs, P. Kamlot, J. Grupa, S. Olivella, and F.D. Hansen, Backfilling and Sealing of Underground Repositories for Radioactive Waste in Salt (BAMBUS-II Project). *Final Report EUR 20621 EN. Luxembourg: Office for Official Publications of the European Community*. ERMS 534716. (2004).

[29] Reda, D.C., Natural convection experiments with a finite-length, vertical, cylindrical heat source in a water-saturated porous medium, *Nuclear and Chemical Waste Management*, 6, 3-14 (1986).

[30] P. Forchheimer, Wasserbewegung durch boden, Zeitschrift Ver. D. Ing., 45 (1901) 1782–1788.

[31] M. Muskat, The flow of homogeneous fluids through porous media, Edwards, MI. (1946).

[32] T. Hayat, F. Hayat, T. Muhammad, A. Alsaedi, Darcy-Forchheimer flow by rotating disk with partial slip, *Appl. Math. Mech. – Engl. Ed.*, 41, 741-752, 2020. https://doi.org/10.1007/s10483-020-2608-9

[33] Sohail Nadeem, Misbah Ijaz, Muhammad Ayub, Darcy–Forchheimer flow under rotating disk and entropy generation with thermal radiation and heat source/sink, *J Therm Anal Calorim.* (2020). https://doi.org/10.1007/s10973-020-09737-1

[34] Anwar Saeed, Asifa Tassaddiq, Arshad Khan, Muhammad Jawad, Wejdan Deebani, Zahir Shah and Saeed Islam, Darcy-Forchheimer MHD Hybrid Nanofluid Flow and Heat Transfer Analysis over a Porous Stretching Cylinder, *Coatings*, 2020, *10*(4), https://doi.org/10.3390/coatings10040391

[35] Keller H.B., Numerical methods in boundary-layer theory, *Ann. Rev. Fluid Mech*. 10, 417-433 (1978).

[36] N. Vedavathi, G. Dharmaiah, S. Abdul Gaffar, K. Venkatadri, Entropy analysis of magnetohydrodynamic nanofluid transport from an inverted cone: Buongiorno's model, ***Heat Transfer Journal***, https://doi.org/10.1002/htj.22021, 2020.

[37] N. Vedavathi, G. Dharmaiah, S. Abdul Gaffar, K. Venkatadri**,** Entropy analysis of Nanofluid magnetohydrodynamic convection flow past an inclined surface: A Numerical review, *Heat Transfer Journal*. 2021. **https://doi.org/10.1002/htj.22159**

[38] Aamar Abbasi, Waseh Farooq, Iqra Riaz, Stagnation point flow of a Maxwell nanofluid containing a gyrotactic microorganism impinging obliquely on a convective surface, *Heat Transfer*, 49(5), 2977-2999, 2020. https://doi.org/10.1002/htj.21756

[39] Muhammad Khairul Anuar Mohamed, Mohd Zuki Salleh, Anuar Ishak, Effects of Viscous Dissipation on Mixed Convection Boundary Layer Flow Past a Vertical Moving Plate in a Nanofluid, *Journal of Advanced Research in Fluid Mechanics and Thermal Sciences*, 69, Issue 2 (2020) 1-18.

[40] P. Ramesh Reddy, S. Abdul Gaffar, B. Md. Hidayathulla Khan, K. Venkatadri, O. Anwar Beg, Mixed Convection flows of tangent hyperbolic fluid past an isothermal wedge with entropy: A mathematical study, ***Heat Transfer Journal***, Vol. 50, Issue 3, pp.2895-2928, 2021. **https://doi.org/10.1002/htj.22011**

[41] Buongiorno J., Convective transport in Nanofluids, *ASME J Heat Trans.*, Vol. 128, Issue 3, pp.240-250, 2006. Doi:10.1115/1.2150834.

[42] Sutton, G., Sherman, A.: Engineering magnetohydrodynamics. Mc Graw Hill, New York (1965).

[43] A. Pozzi, M. Lupo, The coupling of conduction with laminar natural convection along a flat plate, *Int. J. Heat Mass Trans.*, 31, 1807–1814, 1988. http://dx.doi.org/10.1016/0017-9310(88)90195-0

[44] J.H. Merkin, I. Pop, Conjugate free convection on a vertical surface, *Int. J. Heat Mass Trans.*, 39 (1996) 1527–1534, http://dx.doi.org/10.1016/ 0017-9310(95)00238-3

[45] Sadia Siddiqa, Naheed Begum, Md. Anwar Hossain, M.N. Abrar, Rama Subba Reddy Gorla, Qasem Al-Mdallal, Effect of thermal radiation on conjugate natural convection flow of a micropolar fluid along a vertical surface, *Computer & Mathematics with Applications*, 2020. https://doi.org/10.1016/j.camwa.2020.01.011

[46] H. Schlichting, Boundary-Layer Theory, seventh ed., MacGraw-Hill, New York, 1979.

TABLES

Table 1: Comparison of Local skin friction coefficient, C_{fx}

ξ	Local skin friction coefficient, C_{fx}			
	Pozzi and Lipo [43]	Merkin and Pop [44]	Saddiqa *et al.* [45]	Present
0.1	0.014	0.014	0.014	0.012
0.2	0.051	0.051	0.050	0.049
0.3	0.105	0.105	0.104	0.103
0.4	0.172	0.172	0.172	0.171
0.5	0.250	0.250	0.250	0.249
0.6	0.337	0.337	0.336	0.338
0.7	0.430	0.430	0.430	0.429
0.8	0.530	0.530	0.529	0.528
0.9	0.635	0.635	0.634	0.634
1.0	0.741	0.745	0.744	0.743
1.1	0.829	0.859	0.858	0.857
1.2	0.817	0.972	0.975	0.971

Table 2: Values of C_{fx}, C_{fz}, Nu and Sh for different Nb values

Nb	C_{fx}	C_{fz}	Nu	Sh
0.3	0.1755	0.0009	0.1124	0.1555
0.6	0.1759	0.001	0.0989	0.1595
0.9	0.1763	0.001	0.0872	0.1681
1.5	0.1770	0.001	0.0673	0.1770
2	0.1776	0.001	0.0537	0.2013

Table 3: Values of C_{fx}, C_{fz}, Nu and Sh for different Nt values

Nt	C_{fx}	C_{fz}	Nu	Sh
0	0.1748	0.0009	0.1250	0.3013
0.2	0.1752	0.001	0.1165	0.2740
0.4	0.1757	0.001	0.1084	0.2238
0.6	0.1762	0.001	0.1009	0.1806
0.7	0.1764	0.001	0.0973	0.1455

Table 4: Values of C_{fx}, C_{fz}, Nu and Sh for different βe values

βe	C_{fx}	C_{fz}	Nu	Sh
0.1	0.1748	0.0003	0.1107	0.1939
0.6	0.1756	0.0010	0.1109	0.1951
1.5	0.1756	0.0010	0.1114	0.1568
3	0.1771	0.0007	0.1122	0.1621
7	0.1774	0.0004	0.1129	0.1665

Table 5: Values of C_{fx}, C_{fz}, Nu and Sh for different βi values

βi	C_{fx}	C_{fz}	Nu	Sh
0	0.1463	0	0.1106	0.1937
4	0.1477	0	0.1108	0.1945
8	0.1481	0.0001	0.1111	0.1955
16	0.1484	0.0002	0.1114	0.1969
40	0.1486	0.0013	0.1125	0.2023

Table 6: Values of C_{fx}, C_{fz}, Nu and Sh for different Ha values

Ha	C_{fx}	C_{fz}	Nu	Sh
0.1	0.1706	0.0010	0.1108	0.1949
0.4	0.1723	0.0008	0.1120	0.1998
0.8	0.1742	0.0015	0.1136	0.2056
1.3	0.1759	0.0022	0.1158	0.2120
1.8	0.1772	0.0029	0.1182	0.2175

Table 7: Values of C_{fx}, C_{fz}, Nu and Sh for different Ec values

Ec	C_{fx}	C_{fz}	Nu	Sh
0	0.1754	0.0009	0.1139	0.1999
5	0.1776	0.0010	0.0290	0.2764
8	0.1792	0.0010	-0.0316	0.3297
11	0.1812	0.0010	-0.1025	0.3908
15	0.1846	0.0010	-0.2207	0.4890

Table 8: Values of C_{fx}, C_{fz}, Nu and Sh for different Da values

Da	C_{fx}	C_{fz}	Nu	Sh
0.05	0.1257	0.0002	0.1194	0.2462
0.075	0.1531	0.0006	0.1112	0.2271
0.1	0.1755	0.0009	0.1124	0.2013
0.15	0.2112	0.0017	0.1268	0.1644
0.2	0.2398	0.0027	0.1450	0.1474

Table 9: Values of C_{fx}, C_{fz}, Nu and Sh for different Fs values

Fs	C_{fx}	C_{fz}	Nu	Sh
0	0.1758	0.0010	0.1111	0.1993
0.5	0.1726	0.0009	0.1165	0.2076
1	0.1741	0.0009	0.1206	0.2133
1.5	0.1712	0.0009	0.1239	0.2175
2	0.1699	0.0008	0.1268	0.2208

FIGURES

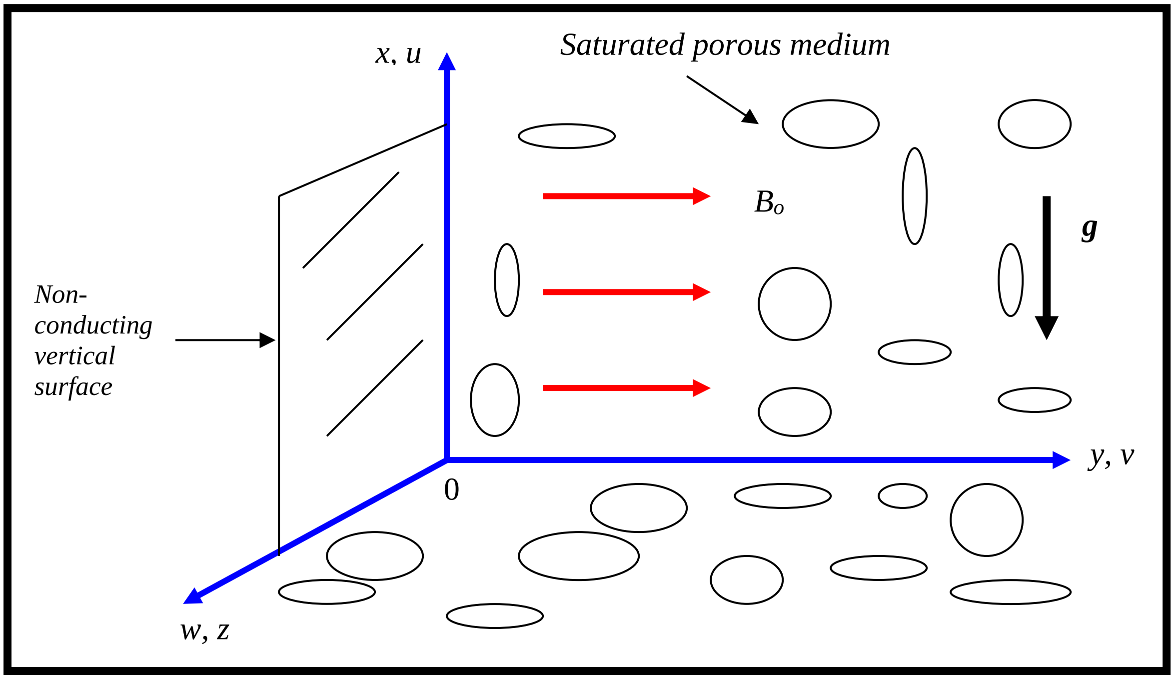

Fig. 1: Physical model and coordinate system

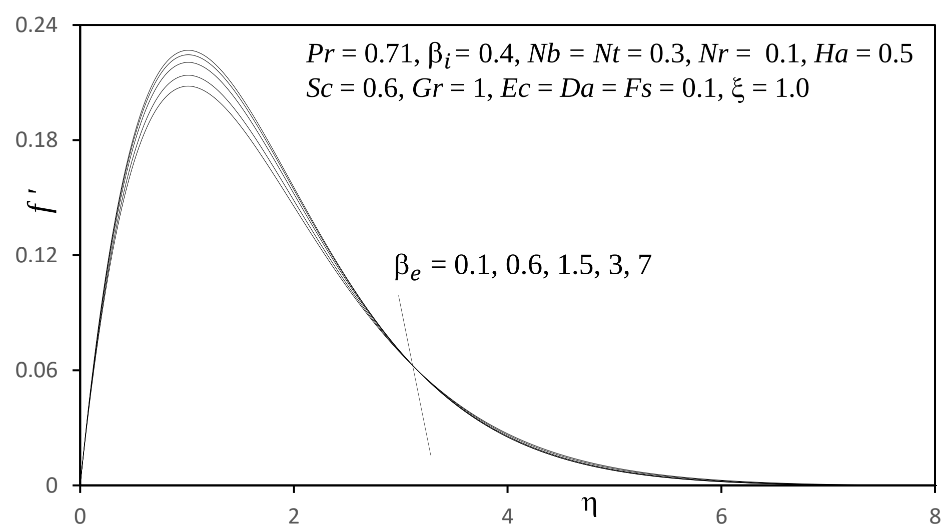

Fig. 2(a) Influence of β_e on Primary Velocity Profiles

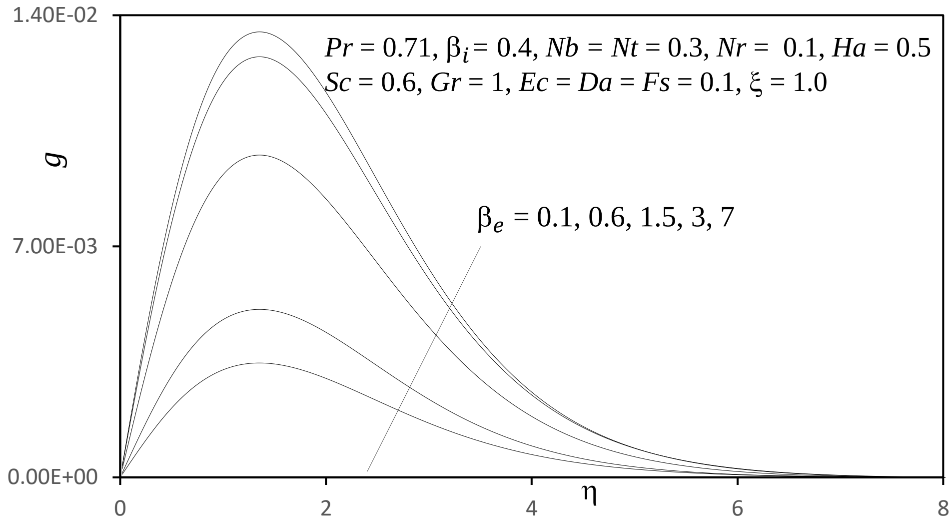

Fig. 2(b) Influence of β_e on Secondary Velocity Profiles

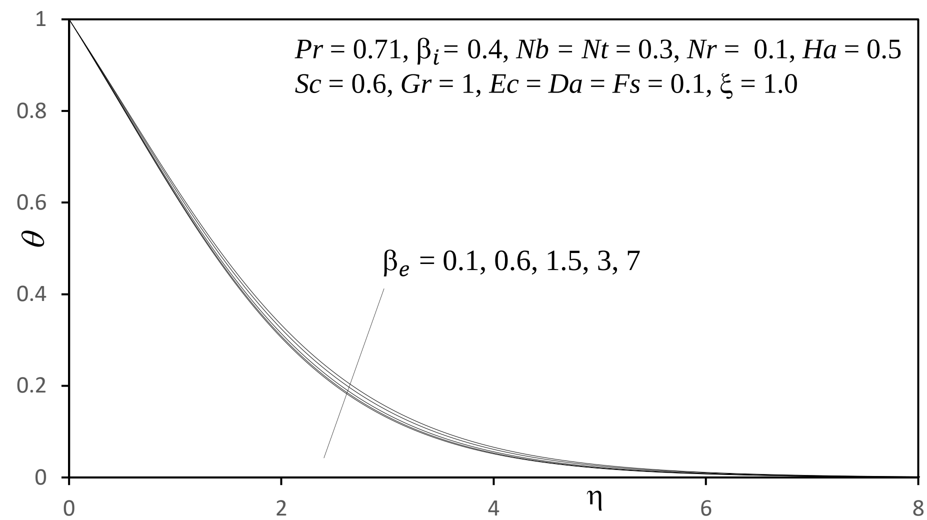

Fig. 2(c) Influence of β_e on Temperature Profiles

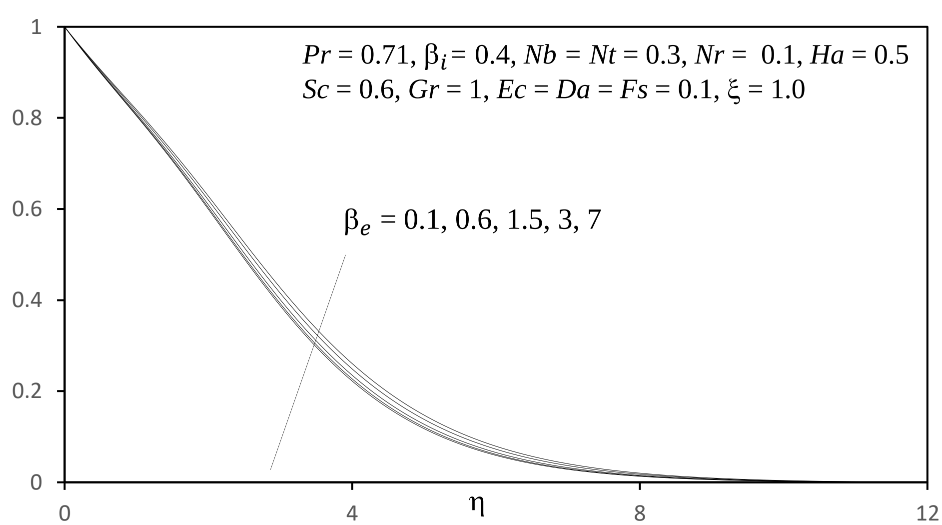

Fig. 2(d) Influence of β_e on Concentration Profiles

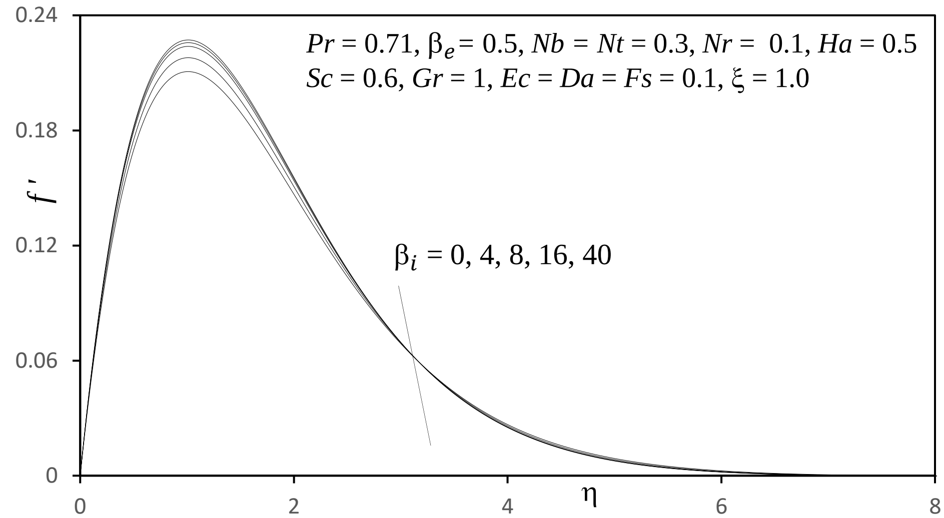

Fig. 3(a) Influence of β_i on Primary Velocity Profiles

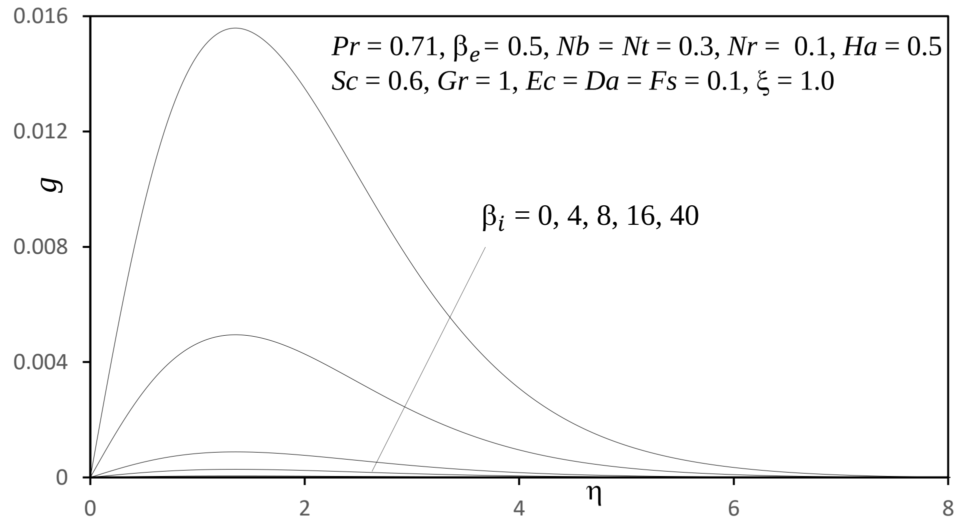

Fig. 3(b) Influence of β_i on Secondary Velocity Profiles

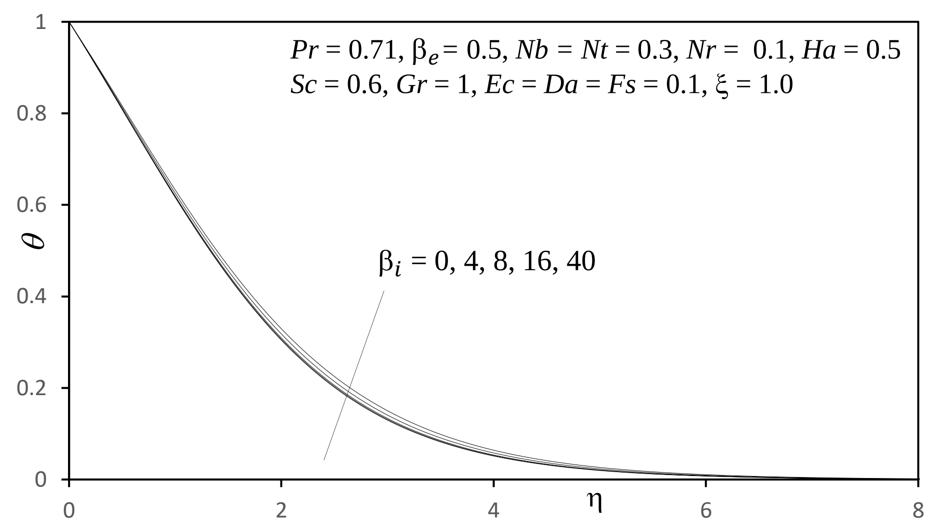

Fig. 3(c) Influence of β_i on Temperature Profiles

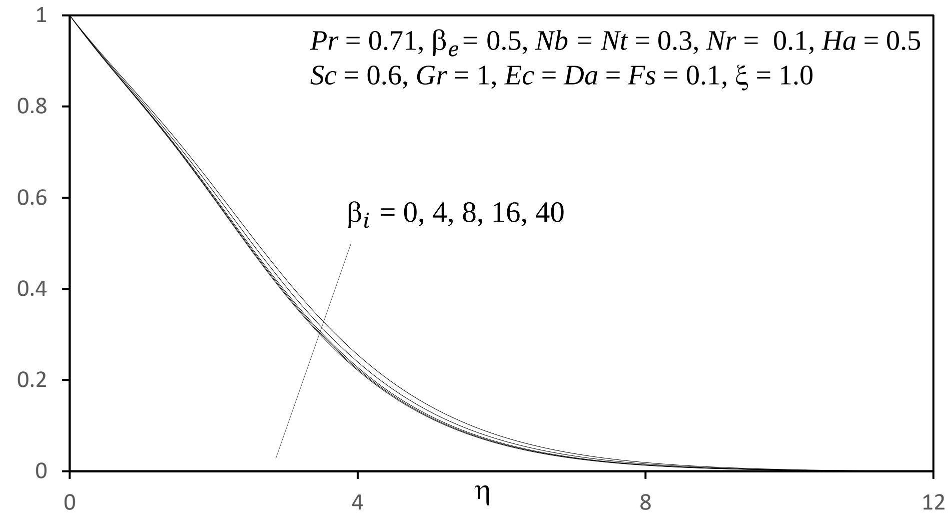

Fig. 3(d) Influence of β_i on Concentration Profiles

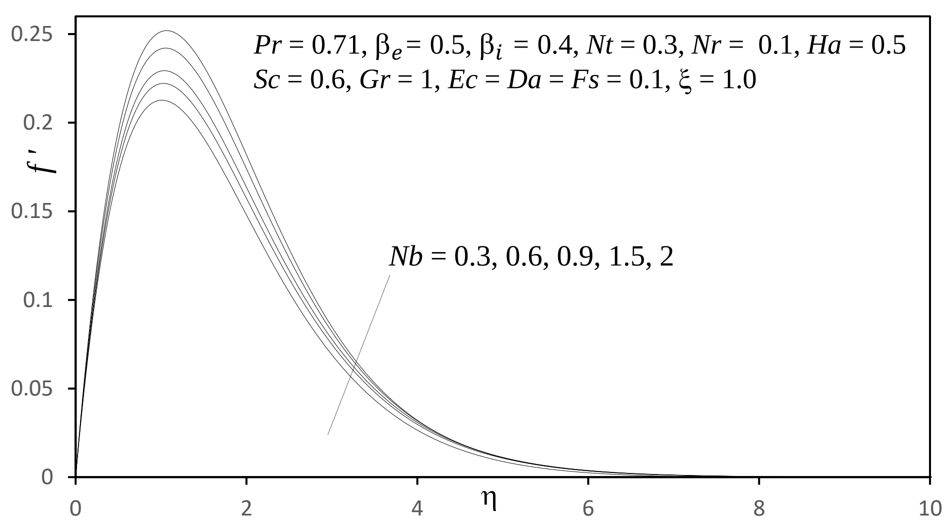

Fig. 4(a) Influence of *Nb* on Primary Velocity Profiles

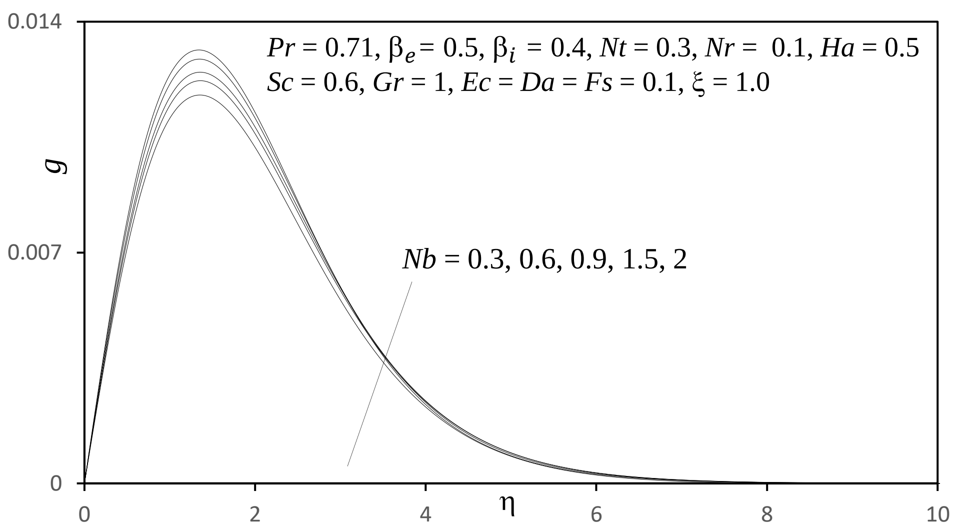

Fig. 4(b) Influence of *Nb* on Secondary Velocity Profiles

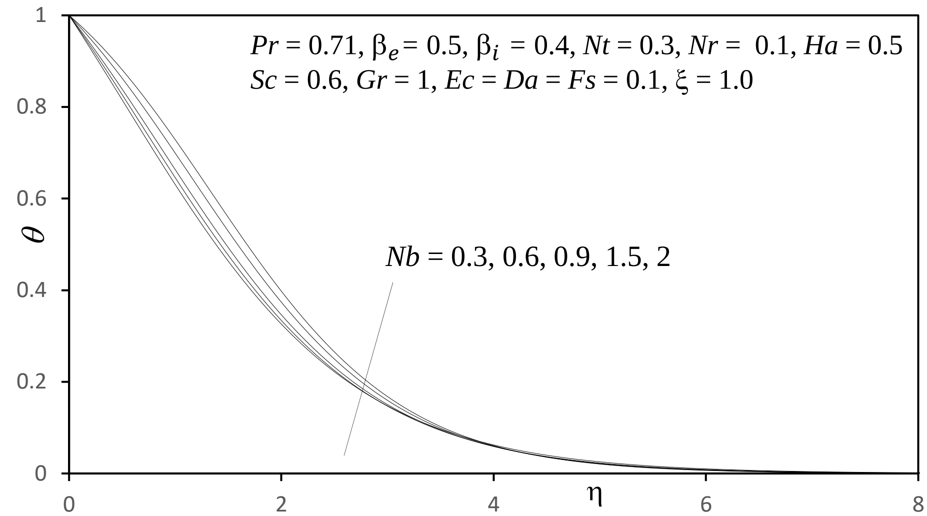

Fig. 4(c) Influence of *Nb* on Temperature Profiles

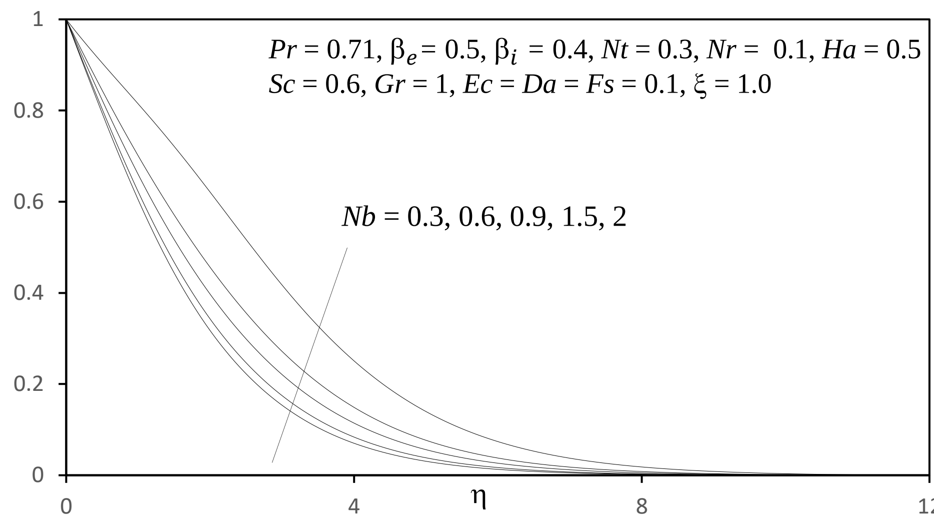

Fig. 4(d) Influence of *Nb* on Concentration Profiles

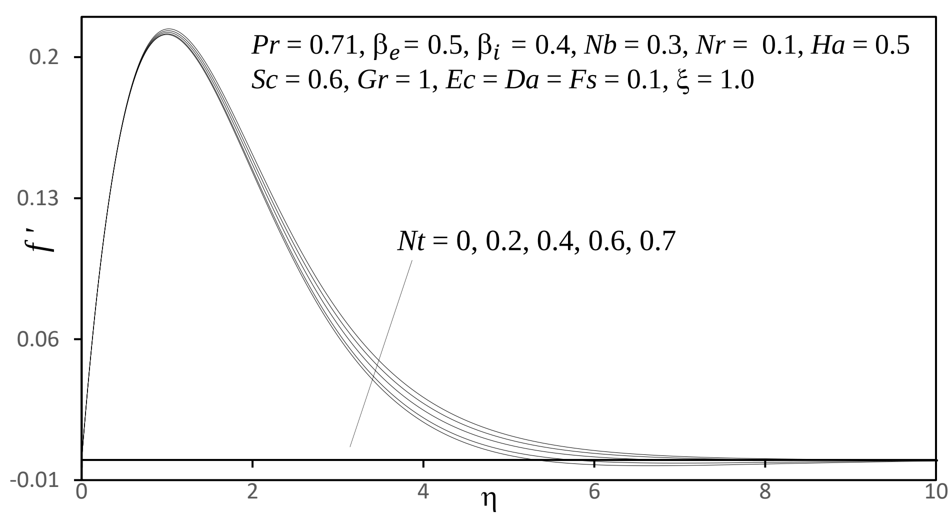

Fig. 5(a) Influence of *Nt* on Primary Velocity Profiles

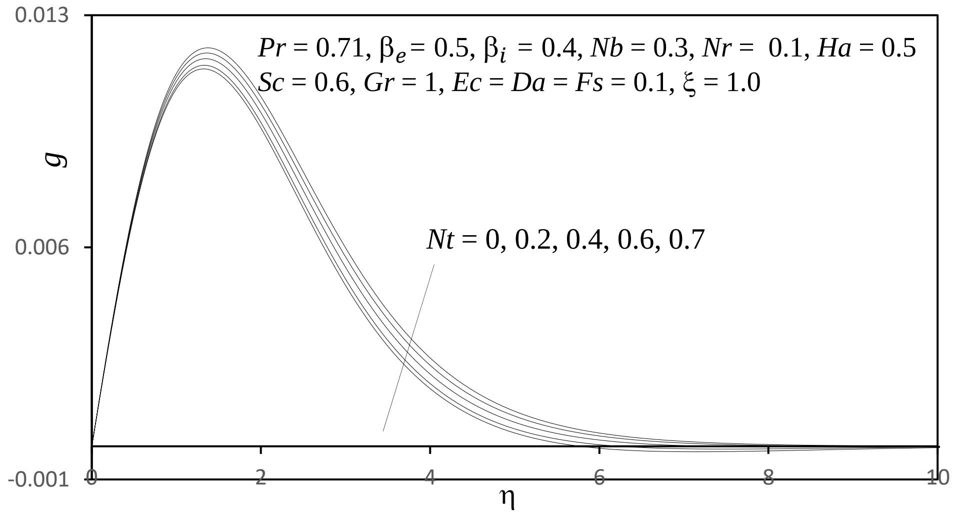

Fig. 5(b) Influence of *Nt* on Secondary Velocity Profiles

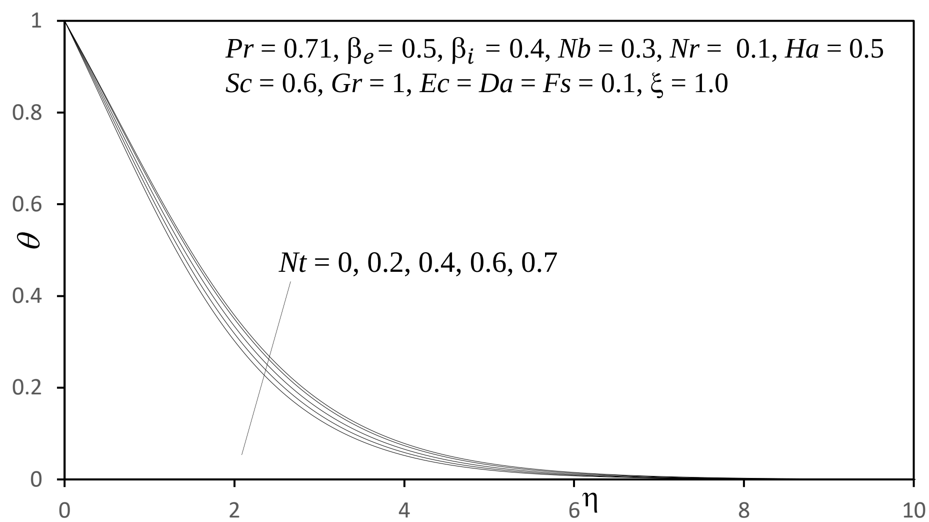

Fig. 5(c) Influence of *Nt* on Temperature Profiles

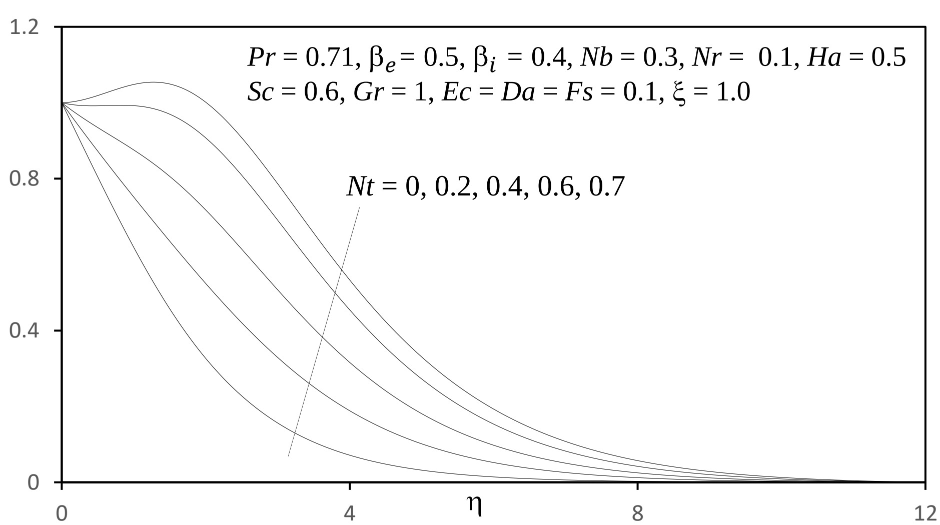

Fig. 5(d) Influence of *Nt* on Concentration Profiles

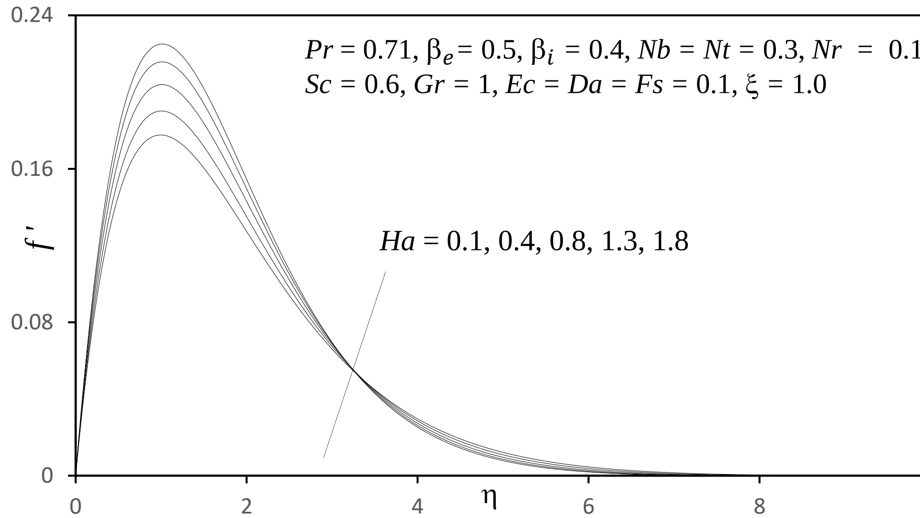

Fig. 6(a) Influence of *Ha* on Primary Velocity Profiles

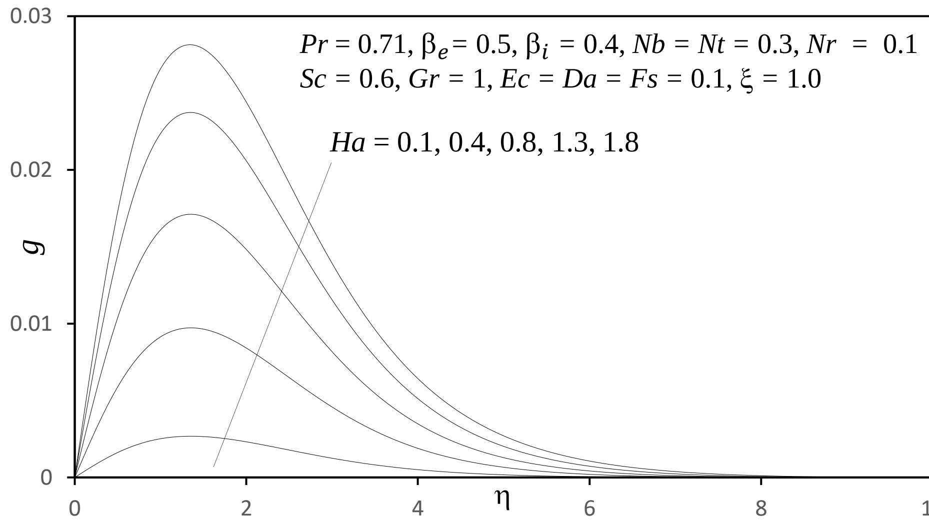

Fig. 6(b) Influence of *Ha* on Secondary Velocity Profiles

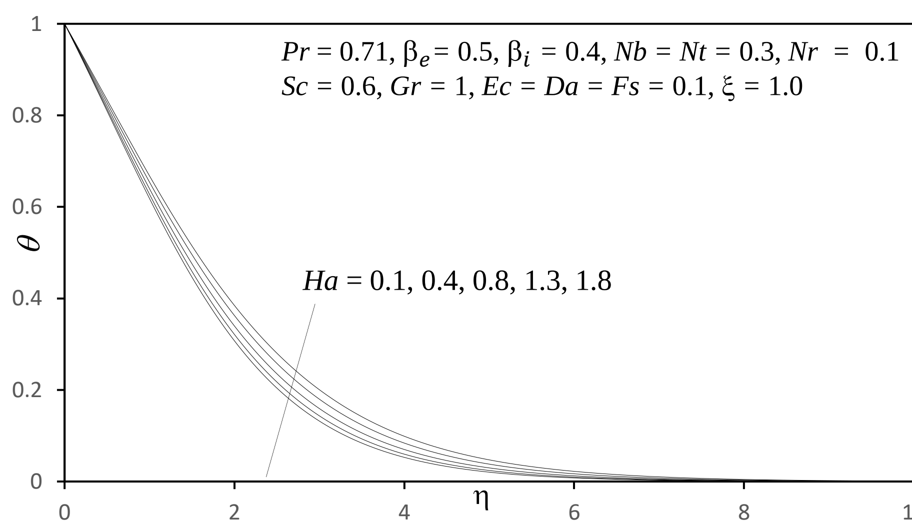

Fig. 6(c) Influence of *Ha* on Temperature Profiles

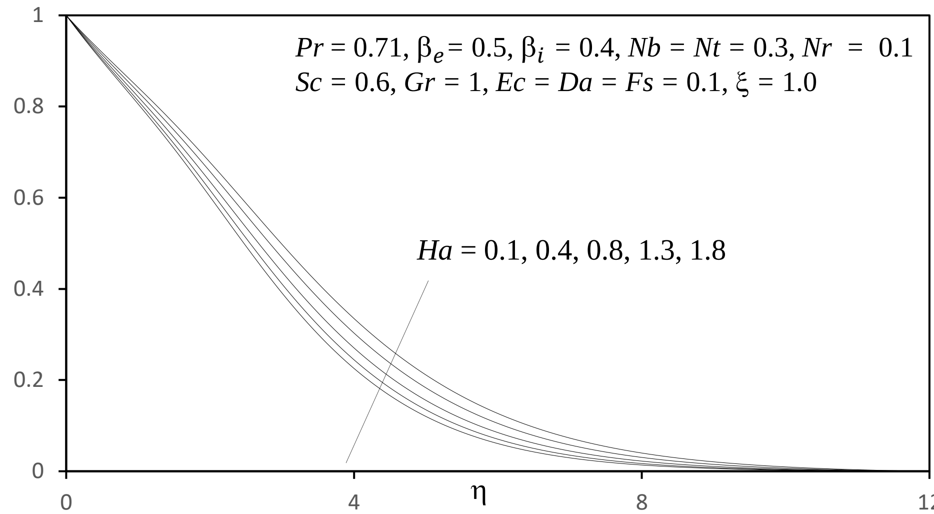

Fig. 6(d) Influence of *Ha* on Concentration Profiles

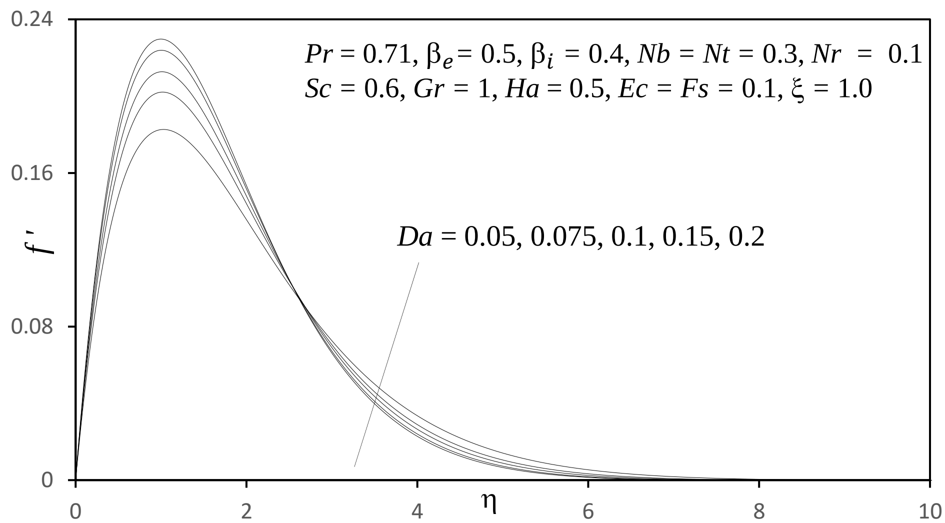

Fig. 7(a) Influence of *Da* on Primary Velocity Profiles

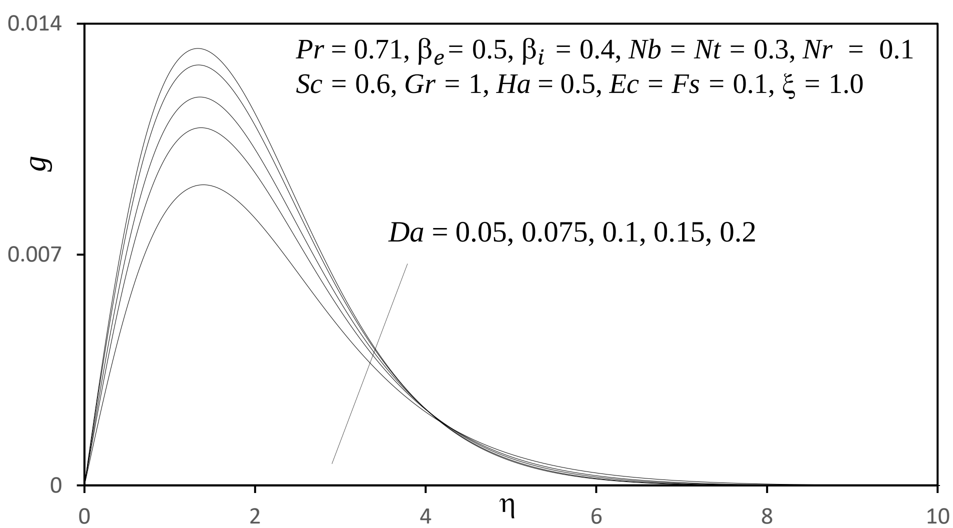

Fig. 7(b) Influence of *Da* on Secondary Velocity Profiles

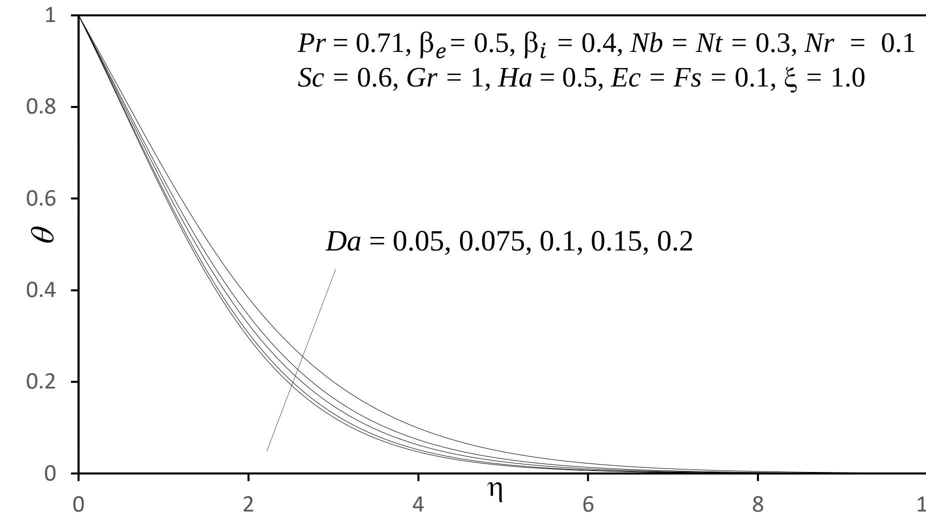

Fig. 7(c) Influence of *Da* on Temperature Profiles

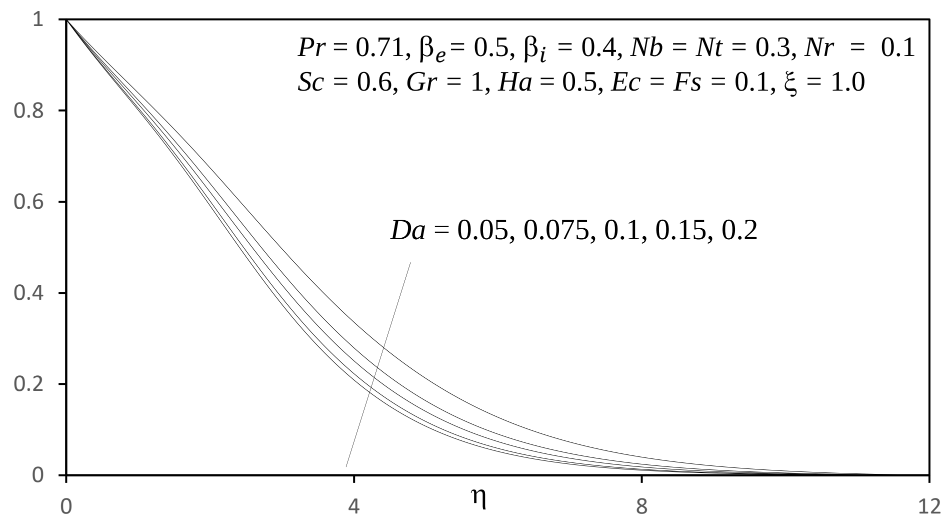

Fig. 7(d) Influence of *Da* on Concentration Profiles

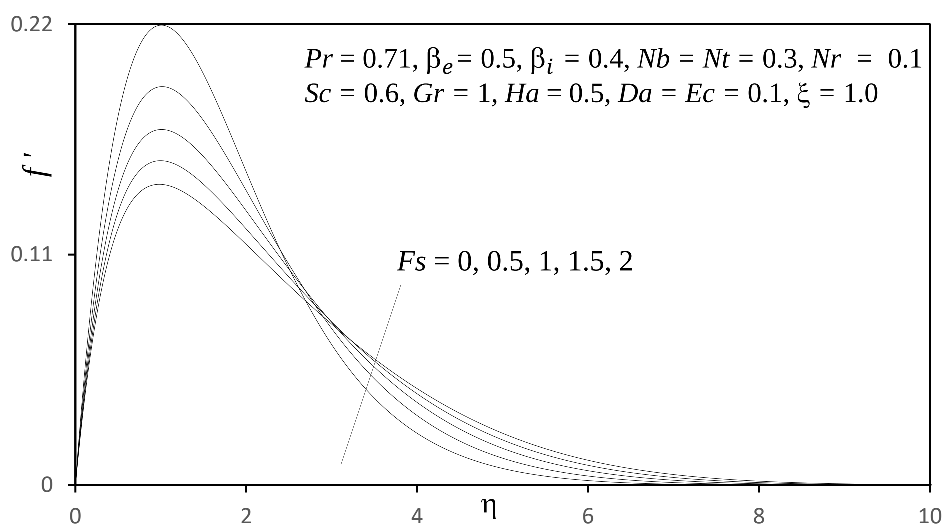

Fig. 8(a) Influence of *Fs* on Primary Velocity Profiles

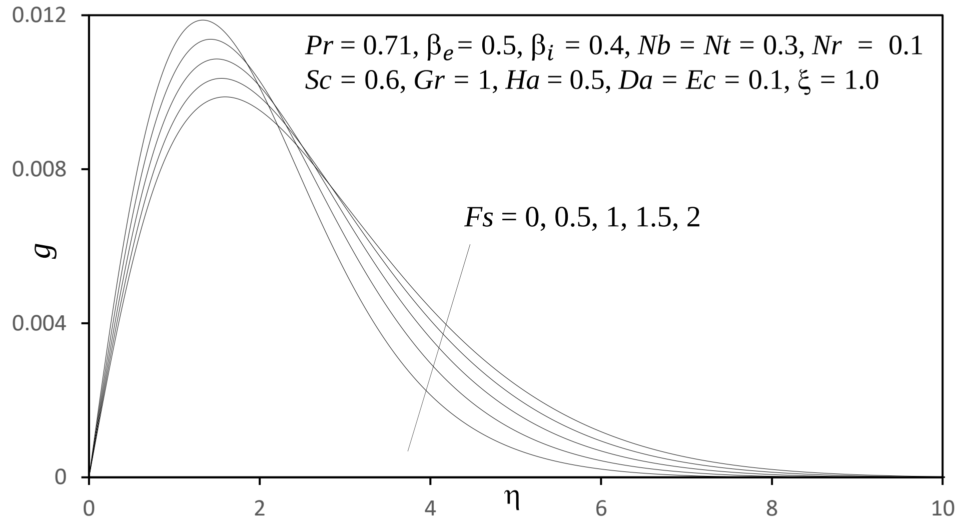

Fig. 8(b) Influence of *Fs* on Secondary Velocity Profiles

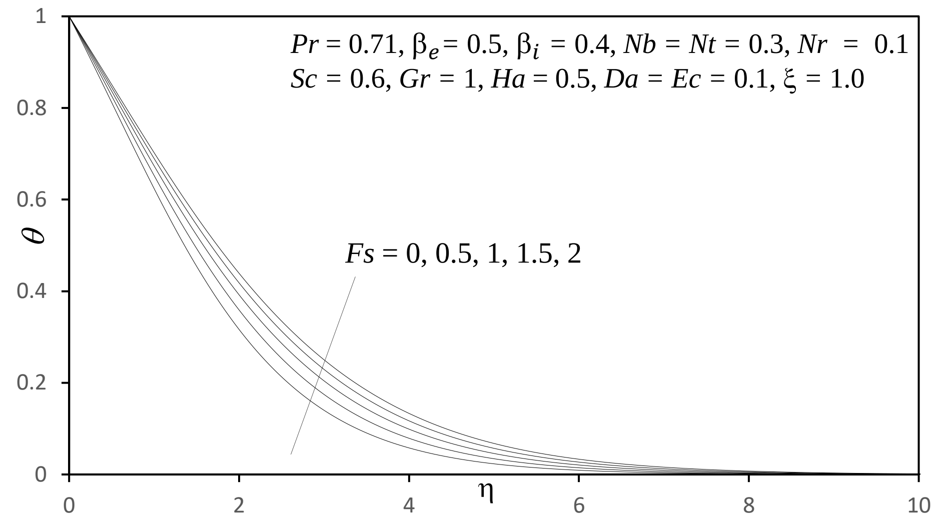

Fig. 8(c) Influence of *Fs* on Temperature Profiles

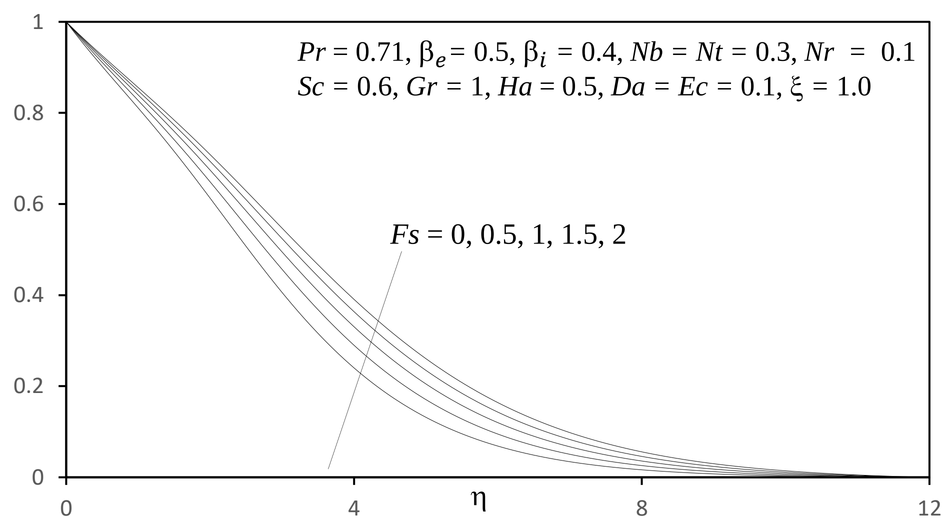

Fig. 8(d) Influence of *Fs* on Concentration Profiles

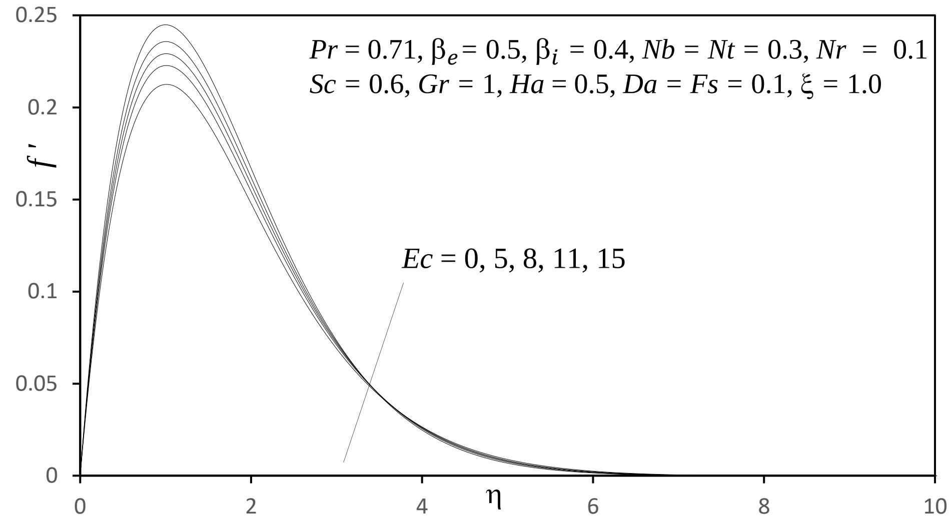

Fig. 9(a) Influence of *Ec* on Primary Velocity Profiles

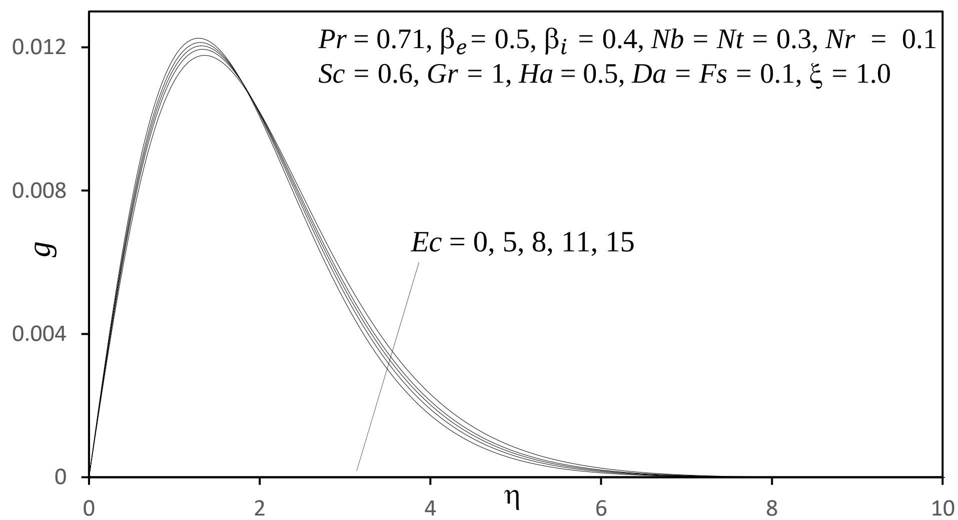

Fig. 9(b) Influence of *Ec* on Secondary Velocity Profiles

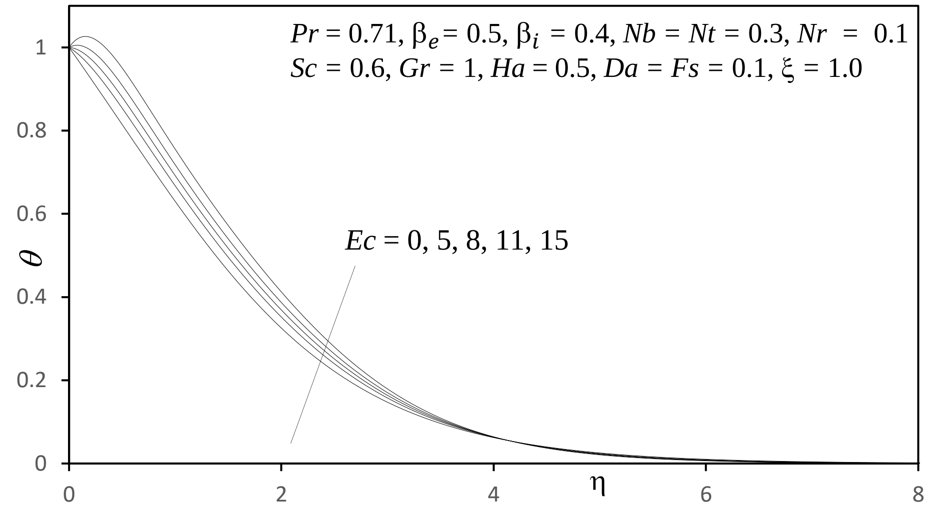

Fig. 9(c) Influence of Ec on Temperature Profiles

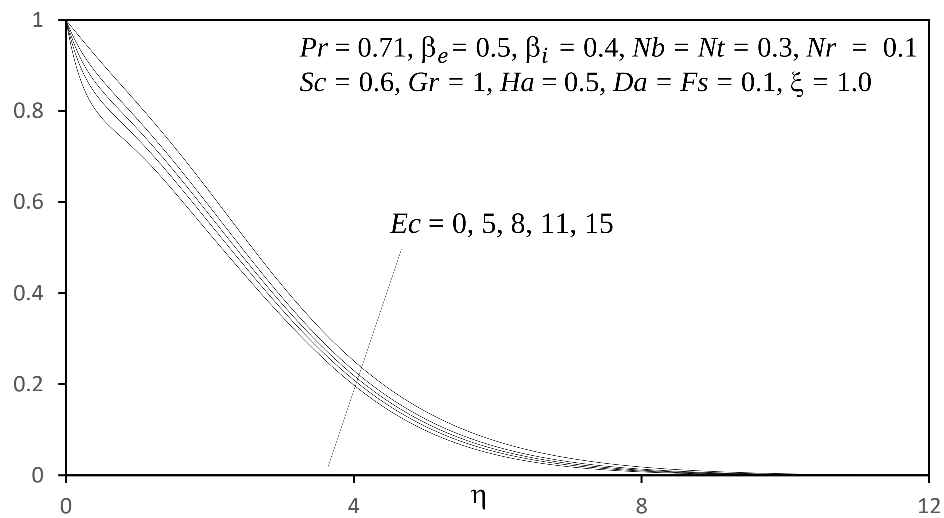

Fig. 9(d) Influence of Ec on Concentration Profiles